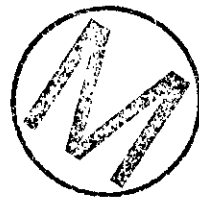


**PEER 2 - Supplementary Information Regarding Conceptual
Models Peer Review**



MEMORANDUM

To: M.G. Marietta
From: T.W. Thompson, F.D. Hansen
Date: July 24, 1996
Subject: Long-term Performance of Panel Closures

**1. INTRODUCTION**

After waste has been emplaced in a panel, closures will be built to restrict flow from the panel during the remainder of the operational phase. These closures will include a length of concrete placed in the panel entries. Although it is not the intent of these closures to restrict flow over the regulatory period of 10,000 years, values for their long-term performance characteristics are required to successfully determine their contribution to overall system performance.

Flow of fluids into or out of the panels will be controlled by the conductance of the panel closure, and of the surrounding disturbed rock zone (DRZ). Performance Assessment (PA) calculations use a constant value for DRZ permeability of 10^{-15} m^2 , a value which is substantiated in the records package for the waste rooms (reference). Consideration of the current panel closure designs indicates that they will maintain their structural integrity for the regulatory period. If this is the case, then the concrete element of the closure system will continue to provide resistance to inward deformation of the surrounding salt, and will prohibit the growth of the DRZ from its initial state. Since the DRZ will not increase during the regulatory period, and may decrease, the assumption of a constant DRZ permeability is reasonable.

The panel closures have been designed to limit the flow of brine and gas between panels during the operational phase, and current designs call for these operational closures to include concrete elements (Figure 1). Although these closures are designed for an operational use, it is expected that they will continue to provide fluid flow restriction during the post-closure phase. The remainder of this memorandum establishes the permeability expectations of the closures, with emphasis on the potential for concrete degradation and increase in permeability. For the purposes of these analyses the concrete elements are taken to have a length of nominally 26 ft (7.9 m) (USDOE, 1996a,b), and to be made of a material chosen so as to be compatible with the environment, such as Salado Mass Concrete (SMC: Sandia, 1996) or a similar mix. Degradation of the concrete may occur by interaction with brine flowing through the plug, or with brines flowing along the plug/salt interface or in the DRZ.

2. CONCRETE PROPERTIES

The initial permeability expected for the concrete panel closures are documented in the materials specification appendix of the Compliance Submittal Design Report (CSDR) (Sandia, 1996) developed for the shaft seal system. In addition to conventional engineering properties, the SMC has well documented permeability characteristics, permeabilities having been determined from field tests (Knowles and Howard, 1996) and laboratory studies (Pfeifle et al., 1996). Figure 2, taken from the CSDR, summarizes the available data, and indicates a permeability for as-placed SMC of between 2×10^{-21} and 1.8×10^{-17} m^2 . For calculations performed in this memorandum a value of 10^{-17} m^2 is used, this being at the high end of the values used by PA for the shaft concrete components, and consistent with other data. For example, data on generic portland cement pastes shows that the permeability of oil field concrete plugs is on the order of 1×10^{-19} m^2 , while data from the Bell Canyon Test indicate permeabilities for borehole concrete plugs of 5×10^{-17} m^2 (Petersen and Christensen, 1980; Christensen and Hunter, 1980).

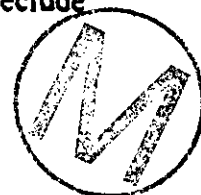
For the purposes of calculating degradation of the concrete member an assumption of porosity is necessary. The expected value is 5%, which is higher than the 2% estimated by Petersen and Christensen (1980) for the Bell Canyon Test plugs, but is generally consistent with practical experience of field emplaced concrete structures, and is the value for cast in-place SMC given in the CSDR (Sandia, 1996). An upper limit for porosity is taken as 10%, which is an engineering estimate for concrete.

As noted in the introduction, the concrete closure member is expected to be structurally stable for the regulatory period, and to provide support for the surrounding rock and the DRZ. In this context it can be noted that the unconfined compressive strength of SMC is greater than 4500 psi (30 MPa), and that under the confined state of stress within the closure system the ultimate strength will be greater than this (Pfeifle et al, 1996). This strength is sufficient to preclude structural failure of the concrete member in the panel entries.

3. DEGRADATION OF CONCRETE

The solid matrix that makes up concrete is composed almost entirely of amorphous to cryptocrystalline solid phases. These phases are thermodynamically unstable, and with time and exposure to water they alter into more stable and more crystalline assemblages. Thermodynamic calculations conducted by Alcorn et al (1992) have predicted the alteration phases of portland cement due to exposure to a variety of waters and brines as including tobermorite, quartz, gypsum, calcite, clays and zeolite, produced at the expense of soluble and unstable materials such as portlandite. The theoretical alteration assemblage occupies more volume than the original solids. These calculated results have been verified by subsequent experiments in which waters and cement were reacted (Onofrei et al., 1992).

At free surfaces concrete materials are not physically supported and can spall. Long term leaching experiments report that surface diffusion controlled alteration is dependent on the C_3A content of the cement and the Mg and SO_4 content of leachant (Walton et al., 1990). Creation of an alteration rind weakens the concrete and makes it subject to spalling (Wakeley et al., 1994). The mechanism for spalling is that the alteration phases occupy more volume than the original



solids, volumetric expansion increases internal pore pressures until concrete tensile strengths are exceeded and spalling occurs. Short-term, empirical studies of ordinary concrete in brine report alteration rates in the range of 0.7 to 1 mm/year (Atkinson and Hearne, 1990) - These rates are likely to be overestimates because diffusion distance varies as the square root of time. Further details are given in Appendix C of Thompson et al., 1996.

4. DEGRADATION OF CONCRETE PANEL CLOSURES



The concrete elements of the panel closures may degrade in one of two ways, either by flow of brines through the mass of the concrete element, or by flow of brines along the interface.

4.1 Flow Through the Concrete Element

An estimate of the degradation of a concrete closure element may be made based on data on the progression of concrete chemical alteration reported by Berner (1990) for both fresh water and brine leachants (Figure 3). The progression is charted in terms of the volume of water flow, and indicates that more than 100 pore volumes of leachants must pass through concrete before there is chemical evidence that the matrix is being attacked. Based on these results, it has been assumed (conservatively) that the concrete closure elements will degrade significantly after 100 pore volumes of water have passed through them. A more detailed discussion of these results is given in Thompson et al. (1996).

This volume can be converted to performance life by using Darcy's Law and considering the flow of fluids through the plug and the surrounding DRZ. If there is a pressure difference between the panel and the rest of the repository, flow will occur through the panel closure and the surrounding DRZ, with the two elements acting as flow resistors in parallel (Figure 4). If the pressure in the panel is P_1 (Pa) and in the rest of repository is P_2 (Pa), then under brine saturated conditions, the steady state flow rate out of the panels will be Q , where:

$$Q = A \cdot (k'/\mu) \cdot (P_1 - P_2) / L \quad \text{m}^3/\text{sec}, \quad (1)$$

where:

- A is the total flow area of the panel closure plus DRZ (m^2)
- L is the flow length (m)
- μ is the fluid viscosity (Pa.s)
- k' is the composite permeability of the panel closure plus DRZ (m^2).

The composite permeability, k' , is given by:

$$k' = (k_d A_d + k_c A_c) / (A_d + A_c), \quad (2)$$

where:

- k_d, k_c are the permeabilities of the DRZ and plug closure respectively (m^2)
- A_d, A_c are the flow cross-sectional areas of the DRZ and plug closure respectively (m^2).

The flow through the panel closure, q_c , will be:

$$q_c/Q = k_c A_c / (k_d A_d + k_c A_c). \quad (3)$$

The pore volume of the panel closure (V_p) is:

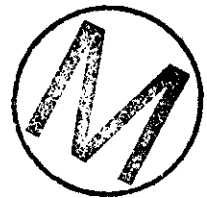
$$V_p = A_c L \phi \text{ m}^3,$$

where ϕ is the porosity. The number of pore volumes (N_p) flowing through the closure in unit time will be:

$$N_p = q_c / V_p \text{ pore volumes/sec,}$$

and the time for 100 pore volumes to flow through the closure will be:

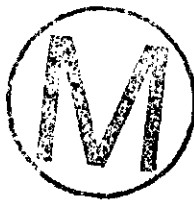
$$t_{100} = 100 / (N_p * 3.154 \times 10^7) \text{ years}$$



The current design (USDOE, 1996a,b) calls for a length of 7.9 m (26 ft) for the concrete closure, and a cross-sectional area of 39.6 m^2 (10 m wide by 3.96 m high). As noted in Section 2 an undegraded concrete permeability of 10^{-17} m^2 , and a porosity ranging from 5% to 10% may be assumed. The DRZ around the closure is assumed to have a permeability of 10^{-15} m^2 . Based on the BRAGFLO grid (reference) the DRZ may be assumed to have a height of 11.95 m above the closure and 2.23 m below. It is assumed that the DRZ in the pillars at either side of the closure heals due to creep closure onto the rigid concrete. The DRZ flow area may therefore be taken as 141.8 m^2 (11.95 + 2.23 m high by 10 m wide).

Given these values, the effective permeability of the closure and the DRZ, from equation (2), is $7.84 \times 10^{-16} \text{ m}^2$, with an effective flow area of 181.4 m^2 . When brine flows between the panel and the rest of the repository, from equation (3), only 0.28 % will flow through the closure, the remainder (99.72 %) will be through the DRZ.

An analysis of calculations made with BRAGFLO (reference) using a range of parameters, and assuming permeabilities for the closures and DRZ of 10^{-15} m^2 , indicates that the maximum cumulative flow between the panel and the rest of the repository for any likely E1 or E2 scenario will be of the order of 10^4 m^3 (Figure 5). With these flows, and the slit in flows indicated above, only 28 m^3 of brine will flow through the concrete closure in 10,000 years. For a porosity range of 5 % to 10 % the maximum cumulative flow through the concrete closure in 10,000 years will therefore be between 0.6 and 1.2 pore volumes. The same point is made in Figure 6, which shows the cumulative flow with closure permeabilities of 10^{-15} to 10^{-17} m^2 . Degradation will be minimal with these flow volumes.



4.2 Flow Along the Interface

Flow along the interface may be more rapid due to the higher permeabilities in the DRZ. A maximum effect of this flow might be estimated to be equivalent to the free surface spall rate of 0.5 to 1 mm/yr. Such a degradation rate is unrealistically high, since the degradation will be controlled by the rate of fluid flow, and total loss of material will not occur in a physically constrained region. However this rate of spall is much less than the expected closure rates (measured at the order of 0.1 to 0.2 ft/yr. or 30 to 60 mm/yr in Panel 1: USDOE, 1996b) so even such a rapid spall rate would be more than compensated for by creep of the salt on the closure. It is therefore concluded that the effect of flow along the interface will be minimal. At most it will lead to an insignificant increase in the DRZ flow area.

5. CONCLUSIONS

It is concluded that the potential flow through the concrete closure is nearly two orders of magnitude too small to cause any significant degradation. Degradation caused by flow in the DRZ adjacent to the concrete will be taken up by creep closure. It is therefore concluded that the panel closures will retain their initial permeability in the post-closure phase. If this permeability is 10^{-17} m^2 , then the effective permeability of the DRZ and the closure together will be about $8 \times 10^{-16} \text{ m}^2$. An assumption of a permeability of 10^{-15} m^2 for the closure and the DRZ is reasonable.

It is also concluded that since no significant degradation is expected for the concrete members, these will maintain their structural integrity and will provide a rigid support to prevent growth of the DRZ during the regulatory period.

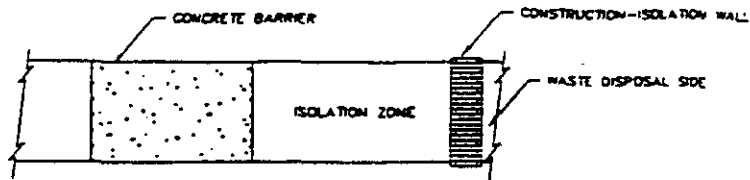
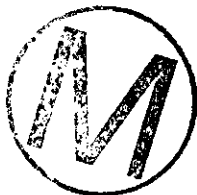
6. REFERENCES

- Alcorn, S.R., Coons, W.E., Christian-Frear, T.L., and M.G. Wallace, 1992, "Theoretical Investigations of Grout Seal Longevity," Final Report, Stripa Project TR 92-23, SKB, Stockholm, Sweden.
- Atkinson, A., Goult, D.J., and Hearne, J.A., 1985, "An Assessment of the Long-Term Durability of Concrete in Radioactive Waste Management." Materials Research Society Symposium Proceedings: Scientific Basis for Nuclear Waste Management IX, v. 50, pp 239-246.
- Berner, U., 1990, "A Thermodynamic Description of the Evolution of Pore Water Chemistry and Uranium Speciation During the Degradation of Cement," Technical Report 90-12, Paul Scherrer, Villigen, Switzerland.
- Bonen, D., 1996, "Petrographic Analyses of Concrete and Grout Recovered from the WIPP," The Technological Institute, Northwestern University, Interim Report, January 15, 1996, 9pp.
- Christensen, C.L. and Hunter, T.O., (1980) "The Bell Canyon Test Results" SAND80-2414C. Sandia National Laboratory, Albuquerque NM

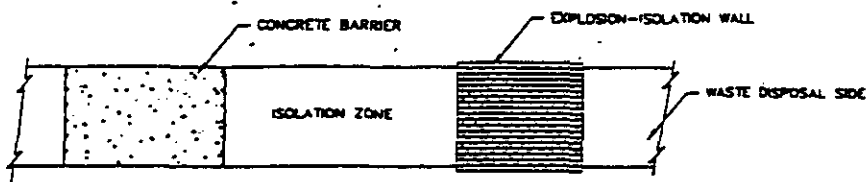
- Knowles, M.K., and C.L. Howard, 1996, "Small Scale Seal Test Results," Waste Management '96, Tuscon, AZ.
- Onofrei, M., Gray, M., Coons, W.E., and S.R. Alcorn, 1992, "High Performance Cement Based Grout for Use in a Nuclear Waste Disposal Facility," Waste Management, v.12, pp. 133-154.
- Petersen, E.W., and Christensen, C.L. (1980) "Analysis of Bell Canyon Test Results" SAND80-7044C. Sandia National Laboratories, Albuquerque NM
- Pfeifle, T.W., F.D. Hansen, and M.K. Knowles, 1996. "Salt-Saturated Concrete Strength and Permeability," 4th. Materials Engineering Conference, ASCE, Washington, D.C.
- Sandia National Laboratories, Repository Isolation Department, 1996. "Compliance Submittal Design Report," Sandia National Laboratories, Department 6121, Albuquerque, NM
- Thompson, T.W., W.E. Coons, J.L. Krumhansl, and F.D. Hansen, 1996. "Inadvertent Intrusion Borehole Permeability," Memorandum of Record, July 8, 1996, Sandia National Laboratories, Albuquerque, NM.
- Wakeley, L.D., Poole, T.S., and Burkes, J.P., 1994, "Durability of concrete materials in high-magnesium brines," SAND 93-7073
- Wakeley, L.D., P.T. Harrington, and F.D. Hansen, 1995, "Variability in Properties of Salado Mass Concrete," SAND94-1495, Sandia National Laboratories, Albuquerque, NM.
- Walton, J.C., Plansky, L.E., and Smith, R.W., 1990, "Models for estimation of service life of concrete barriers in low-level waste repositories," NUREG/CR-5542
- U.S. DOE (Department of Energy), 1995, "Waste Isolation Pilot Plant Sealing System Design Report," DOE/WIPP-95-3117.
- U.S. DOE (Department of Energy), 1996a, "Detailed Design Report for an Operational Phase Panel-Closure System," DOE/WIPP-96-2150.
- U.S. DOE (Department of Energy), 1996b, "Final No Migration Variance Petition," DOE/CAO-96-2160.

BRAGFLO grid (ref)

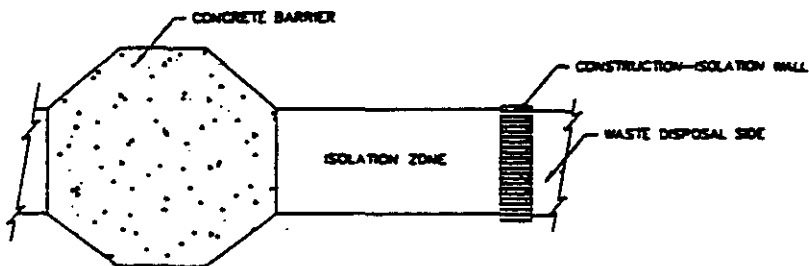




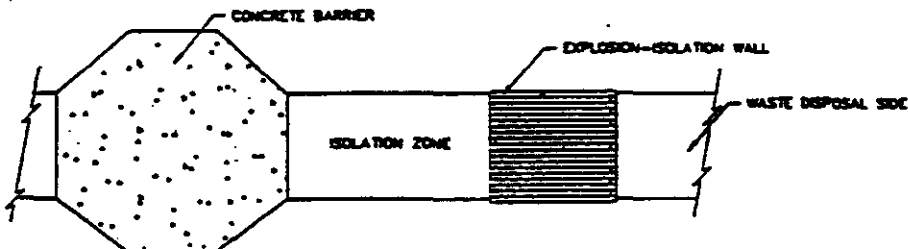
A. CONCRETE BARRIER WITHOUT DRZ REMOVED AND CONSTRUCTION ISOLATION WALL



B. CONCRETE BARRIER WITHOUT DRZ REMOVED AND EXPLOSION ISOLATION WALL



C. CONCRETE BARRIER WITH DRZ REMOVED AND CONSTRUCTION ISOLATION WALL



D. CONCRETE BARRIER WITH DRZ REMOVED AND EXPLOSION ISOLATION WALL

Figure 1: Panel Closure Designs (after USDOE, 1996a)

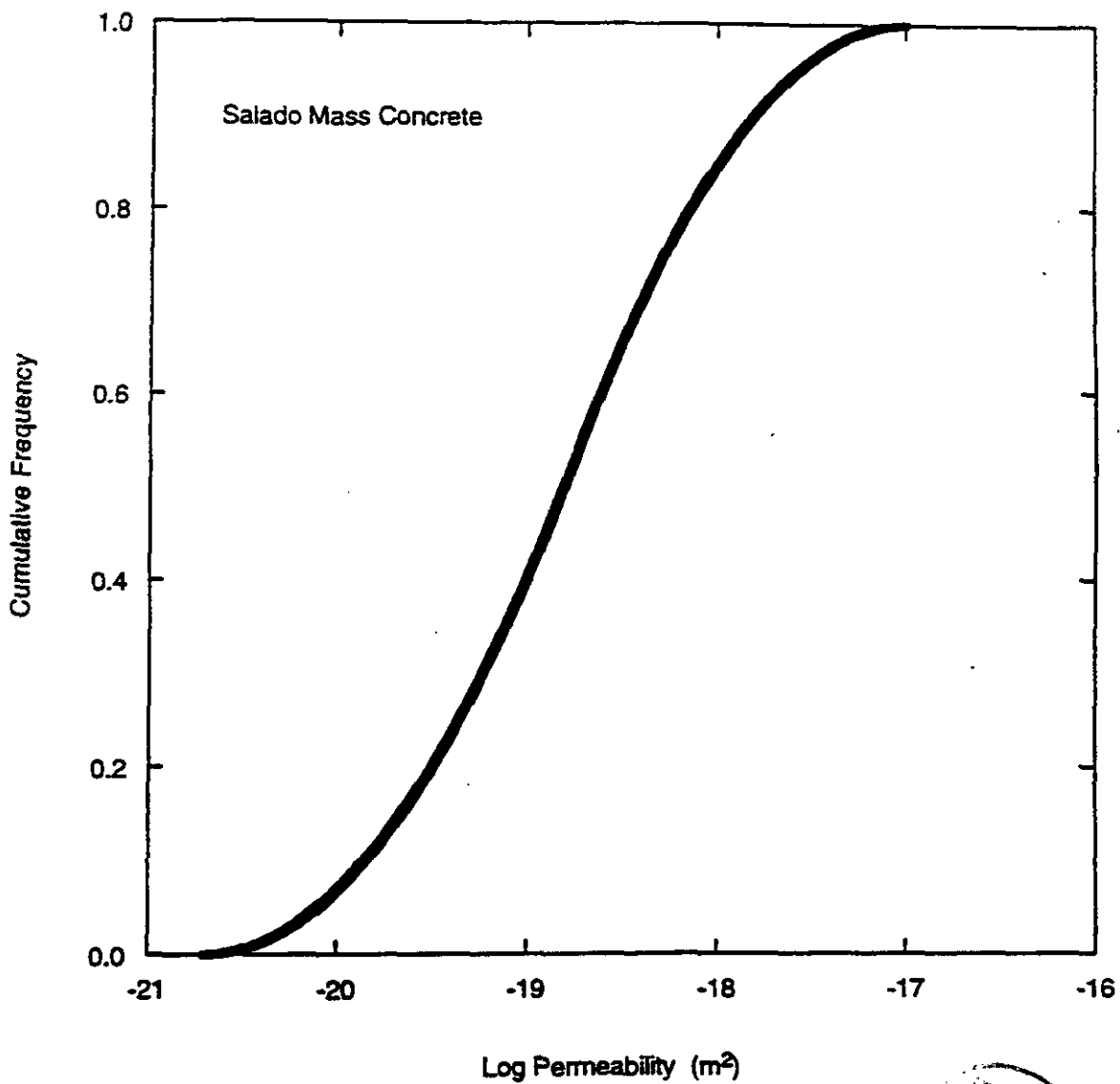


Figure 2: Cumulative Distribution Function for Permeability of SMC (after Sandia, 1996)



Figure c-3 Degradation of "HTS" in standard marl groundwater "MAR". After 6650 cycles calcite is the only solid phase present ($T = 25\text{ }^{\circ}\text{C}$).

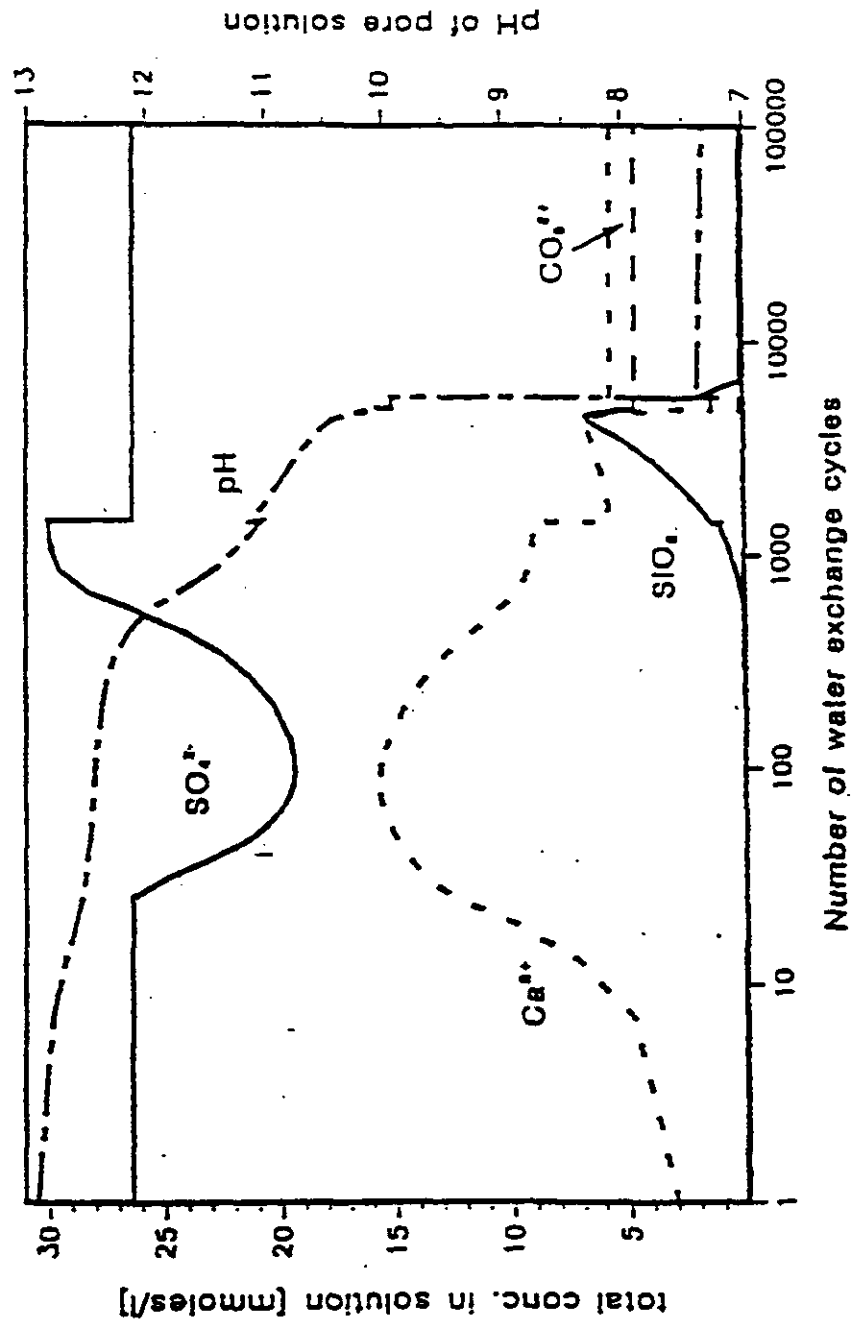


Figure 3: Degradation of Concrete in Brine (after Berner, 1990)

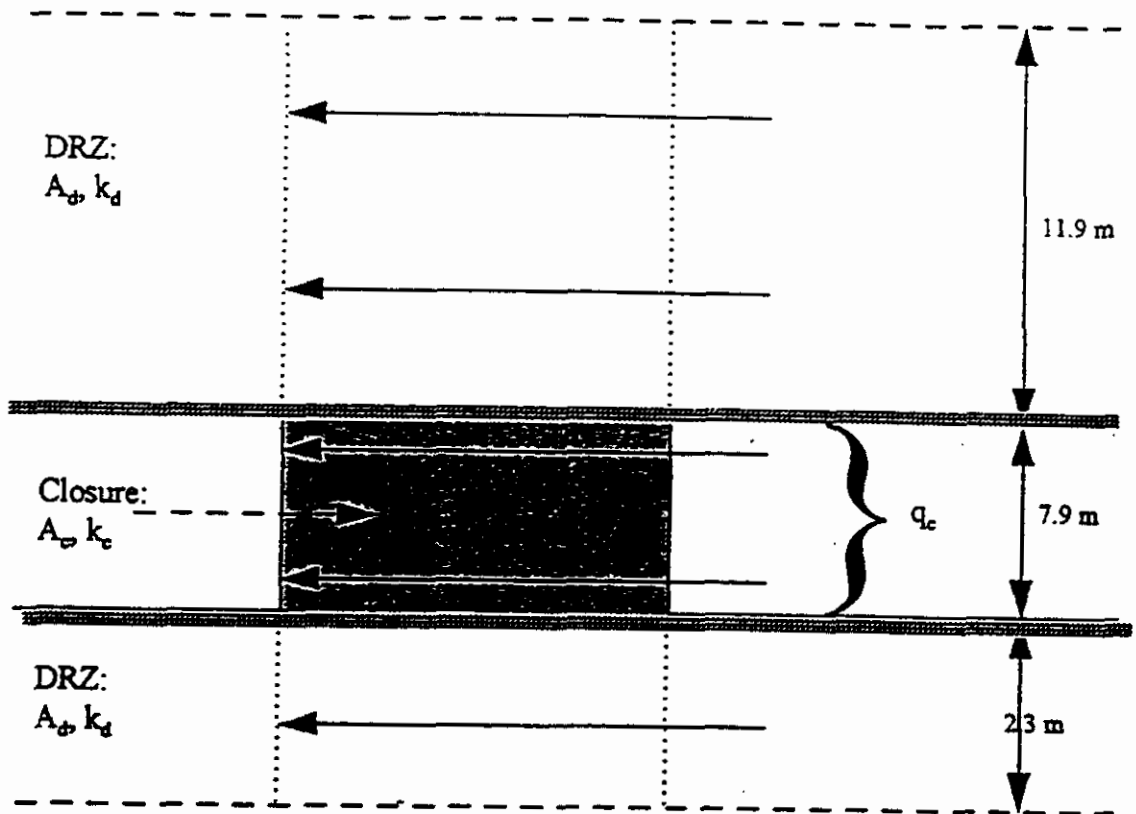


Figure 4: Parallel Flow through the Panel Closure and DRZ

SNL WIPP PA96: BRAGFLO SIMULATIONS (CCA R1 S3)

Cumulative Brine Flow across Panel Seal out of Waste Panel

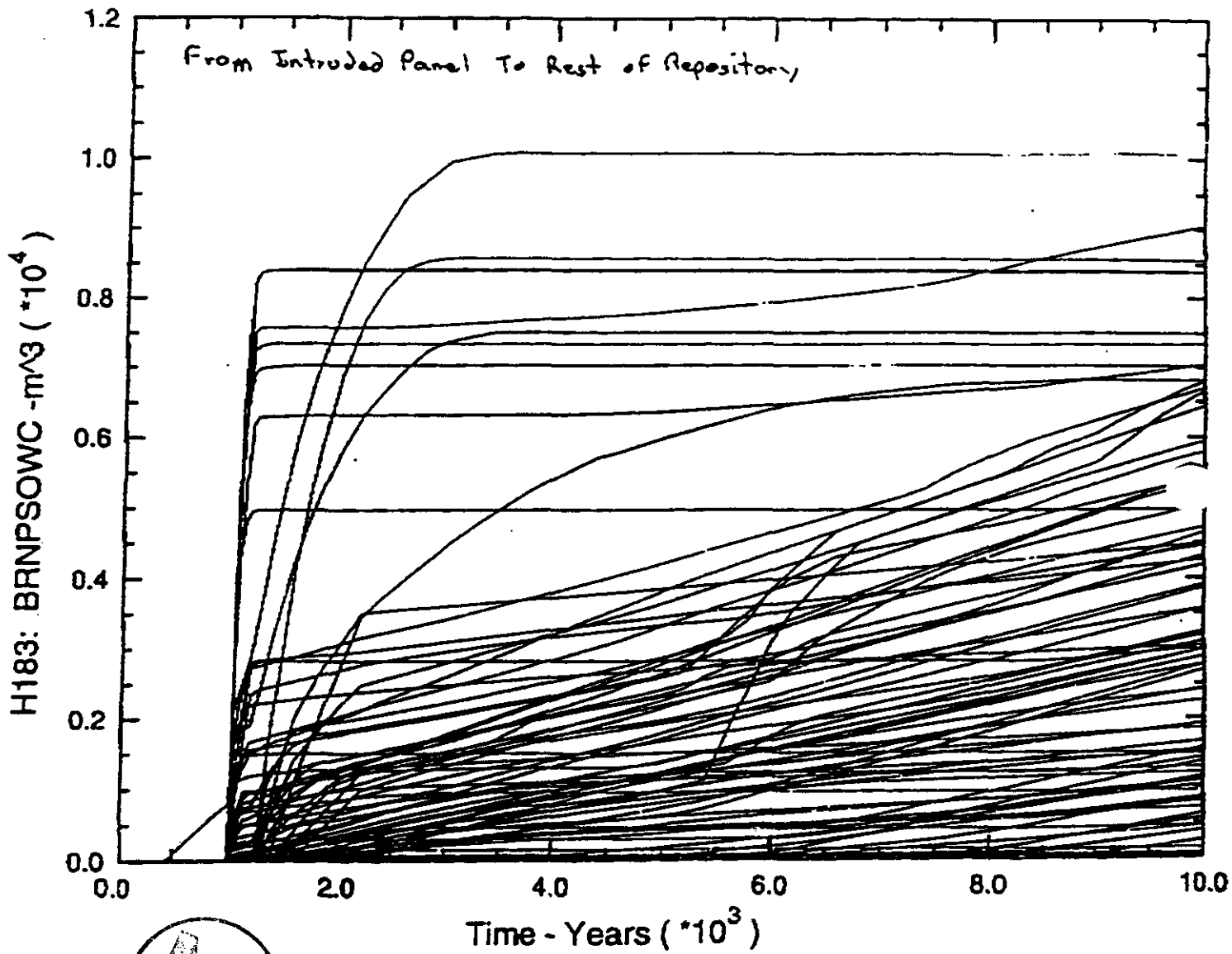


Figure 5: Cumulative flows between a panel and the rest of the repository for an E1 Intrusion at 1000 Years

SNL WIPP PA96: BRAGFLO SIMULATIONS (CCA R1 S3 Vector 25)

Net Brine Inflow across Panel Seal into Rest of Repository

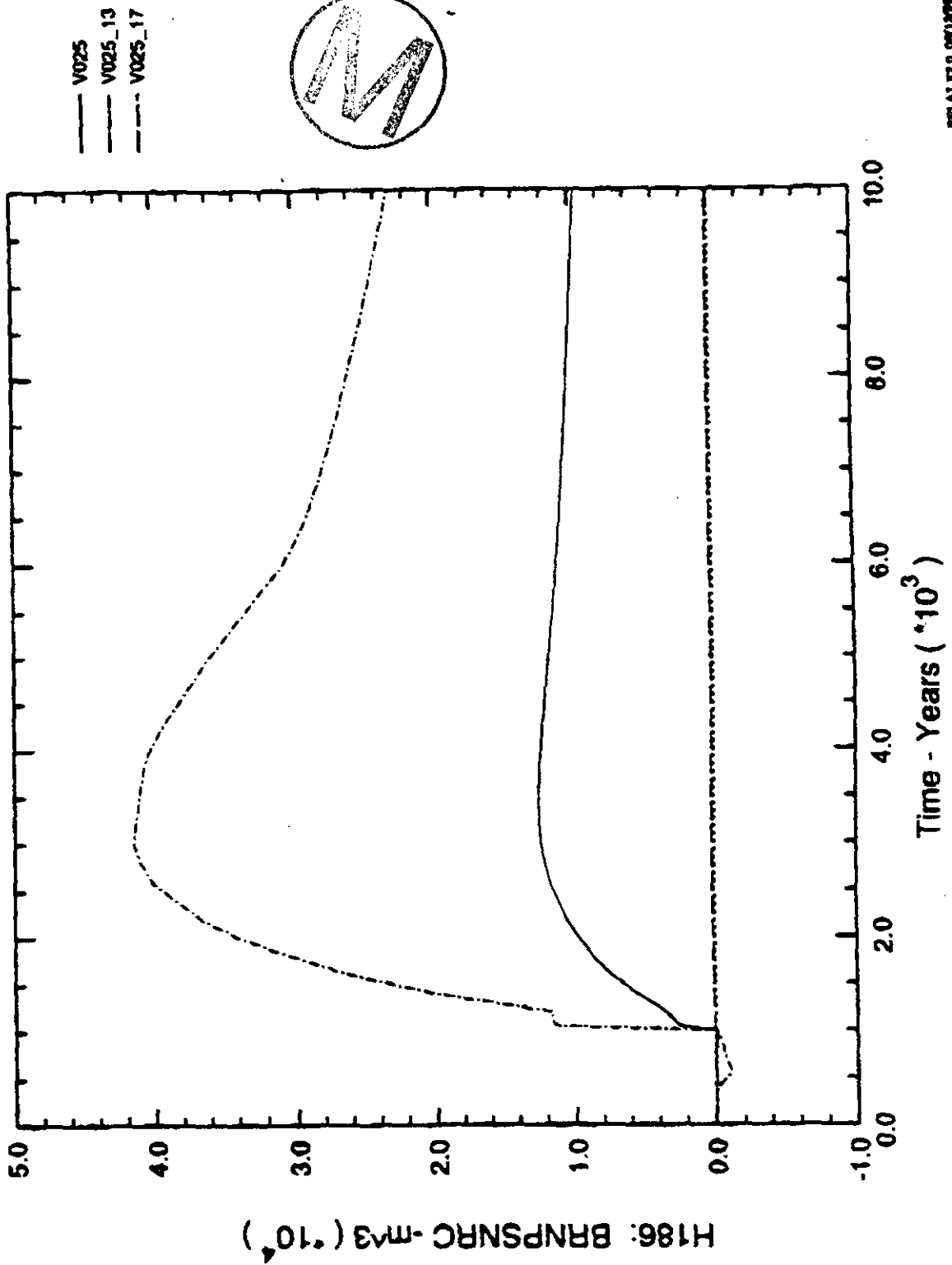


Figure 6: Cumulative flows through the Panel Closures for Permeabilities of 10^{-15} to 10^{-17} m^2 . Results shown are for the Maximum Flow Case of Figure 5.

From: Kurt W. Larson
 To: melord, pvaughn, msychu
 Date: 1/24/96 8:24am
 Subject: Fracture model ideas

A couple of ideas as the frac. model parameters are determined. I will be away next week, so Palmer you will have to see that the memo for Project office to consider gets written.

From brine-outflow meeting 1/23/96:

Wolfgang Wawersik thinks each interbed has a zone about 10cm thick which dilates. Each zone dilates identically. This means a different set of fracture parameters would be applied to each interbed. He and Norm Warpiniski think the LEFM model is appropriate analogous. LEFM predicts about 1 cm dilation max with tremendous permeability change for pressures somewhat above lithostatic.

For MB 138 and 139, 1 cm dilation - 1% porosity change over entire thickness
 For anh.A-B, 1 cm dilation - 3-5% porosity change over entire thickness (someone who knows modeled thickness can figure out more accurately)

dilation/fracturing begins is a continuous process, so initiation pressure should be low.

Additionally, Norm thinks pressures above 17-18 MPa are not realistic, and indicate too constrictive fracture model conditions. Thus, fracture model must be able to open up better than recent implementations (FEAs) which allowed pressures up to 23 MPa.

This leads me to the following recommendation:

Initiation pressure
 about 0.2 MPa above initial pressure of cell

I
 Final Pressure, Final Porosity, Final Permeability
 I suggest using these as fitting parameters so that the following condition is attained

At about 2.5 MPa above initial pressure in cell, fracture porosity and permeability begin steep rise (commensurate with onset of real fracturing) - below this pressure shallower rises indicate interconnection/dilation of existing fractures

a. At about 3 MPa above initial pressure in cell, fracture porosity reaches 1% for MB 139, MB 138; 3-5% for AnhA+B.

b. At about 3 MPa above initial pressure in cell, fracture permeability reaches 8% OM greater than initial.

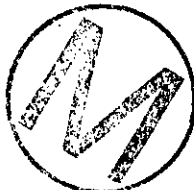
a+b above make a fracture that is relatively long due to high permeability and narrow due to moderate increase in porosity. condition of a+b is ideal max pressure for model, and commensurate with LEFM model.

Above about 3 MPa increase, fracture porosity and permeability continue steep rise so that increased pressures have a mechanism for blowing off steam rapidly.

If the model is set so that there is no increased porosity or permeability above about + 3 MPa, then I think some vectors will result in pressures significantly in excess of 20 MPa.

I look forward to hearing what the final values chosen are

Kurt



Date: 1/29/96

To: Margaret Chu, Dept. 6801, MS-1325

From: Michael Lord, Dept. 6749, MS-1328

Subject: Parameters describing the variable porosity and permeability within anhydrite material.

I have considered ways of honoring the porosity/permeability response to pressure within the anhydrite marker beds as suggested in the enclosed memo from Kurt Larson of 1/24/96 and discussions with Palmer Vaughn. The following values typical of the performance assessment data were assigned:

pressure at fracture initiation	= 12.7 MPa
pressure at full fracture condition	= 16.5 MPa
porosity at reference condition	= 0.011 (1.1%)
permeability of intact anhydrite	= $2.5E-19 \text{ m}^2$
permeability at full fracture condition	= $1.0E-09 \text{ m}^2$

The porosity at full fracture condition was then adjusted in order to produce a change in porosity of about 1% at 2.5 MPa above fracture initiation pressure or a pressure of 15.2 MPa. This was obtained with a maximum porosity of 0.05(5%). In the attached Fig. 1 the resulting porosity response is shown. The corresponding permeability response is shown in Fig. 2. At 2.5 MPa above fracture initiation pressure, the permeability is between 3 and 4 orders of magnitude larger than the intact value. This would represent the desired response in marker beds 138 and 139. A similar analysis was done for marker bed a+b where the full fracture porosity was taken to be 0.25 (25%). For this value of maximum porosity the porosity at 2.5 MPa above fracture initiation pressure is approximately 3% above the porosity at fracture initiation pressure. This is shown in Fig 3 and the result is in line with the proposed response. Fig. 4 shows the permeability at 2.5 MPa above fracture initiation pressure as approximately 4 orders of magnitude above the intact permeability.

Based on this study I would recommend assigning the fracture parameters as follows. The fracture initiation pressure should be set as done in the FEPs calculations where it is assigned a value of 0.2 MPa above the grid block initial pressure. Therefore, there could be some small variance in the fracture initiation pressure if the reference initial pressure in the Salado is sampled. Also, there will be some small variance due to the dip in the Salado formation. However, the fracture initiation pressures should be near the 12.7 MPa value. The pressure at the full fracture condition should be an increment of 3.8 MPa above the fracture initiation pressure. This would result in a full fracture pressure of approximately 16.5 MPa. The full fracture permeability can be any large sampled or assigned value such as the $1.0E-09 \text{ m}^2$ used in this study. The full fracture porosity for the marker beds 138 and 139 will have value 0.05 and the full fracture



porosity for the marker bed a+b will have value 0.25. With these values the pressure dependent porosity and permeability should closely approximate the LEFM predicted values.



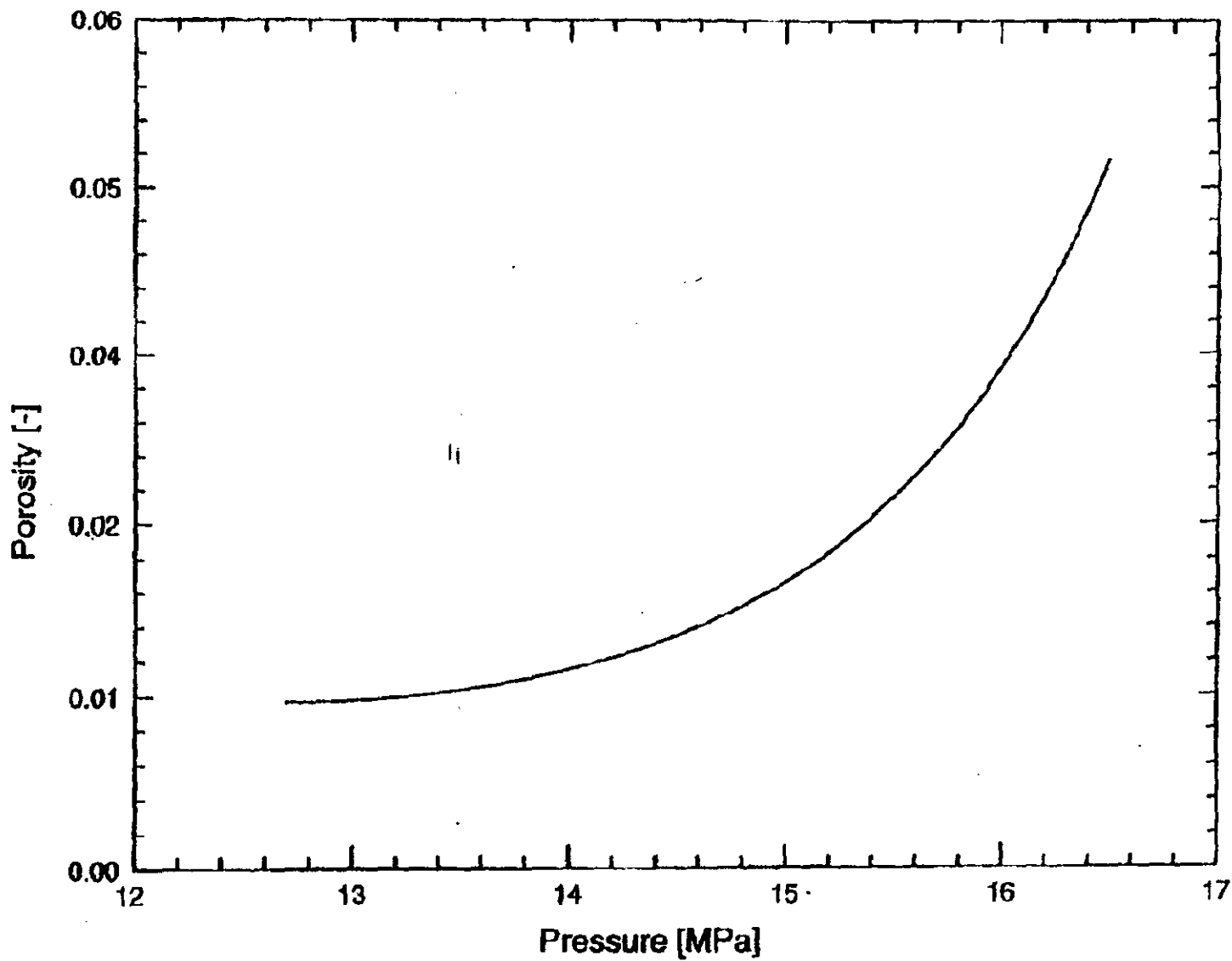


Figure 1: Porosity in Marker Bed 138 & 139 with Fracturing

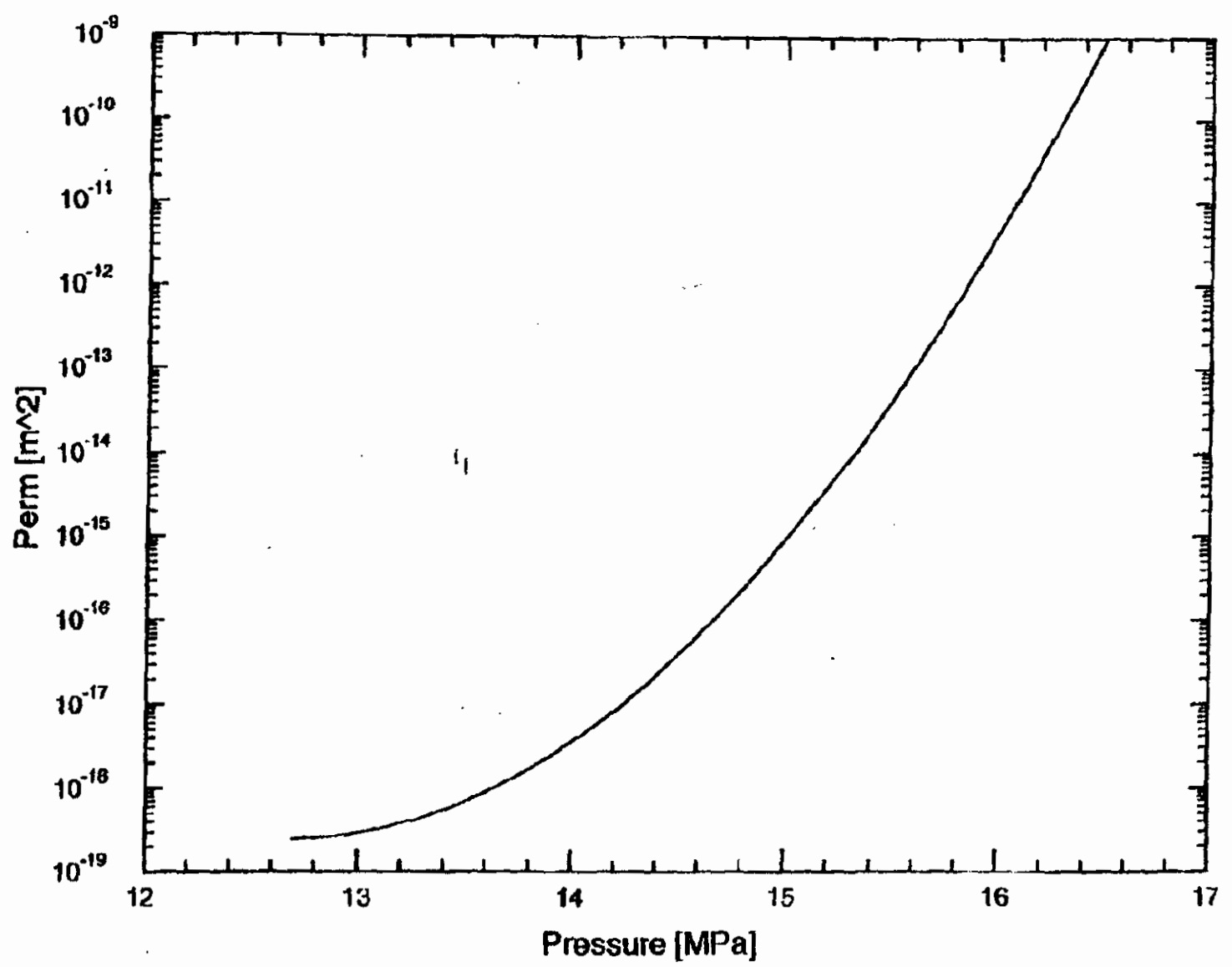


Figure 2: Permeability in Marker Bed 138 & 139 with Fracturing

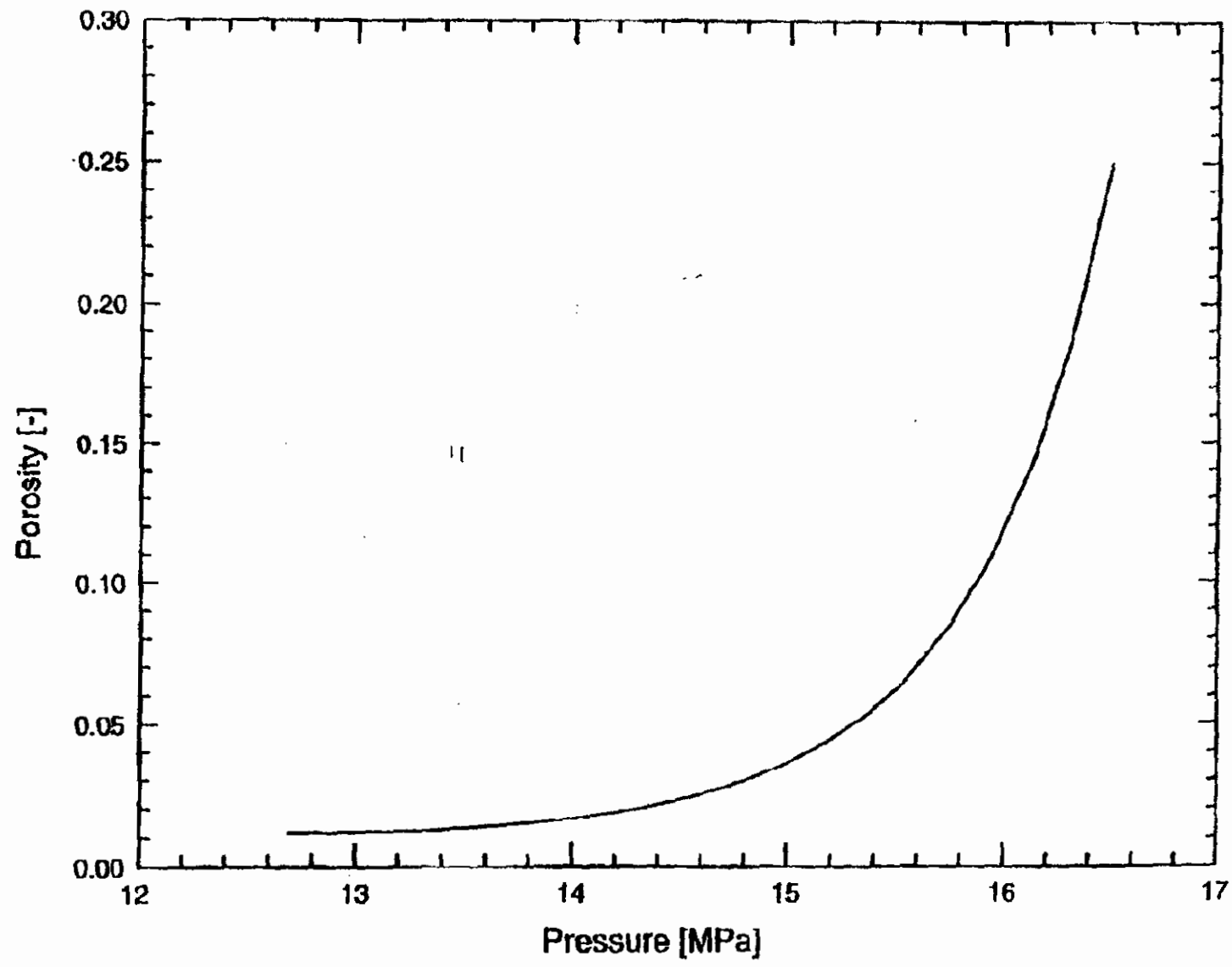


Figure 3: Porosity in Marker Bed A+B with Fracturing



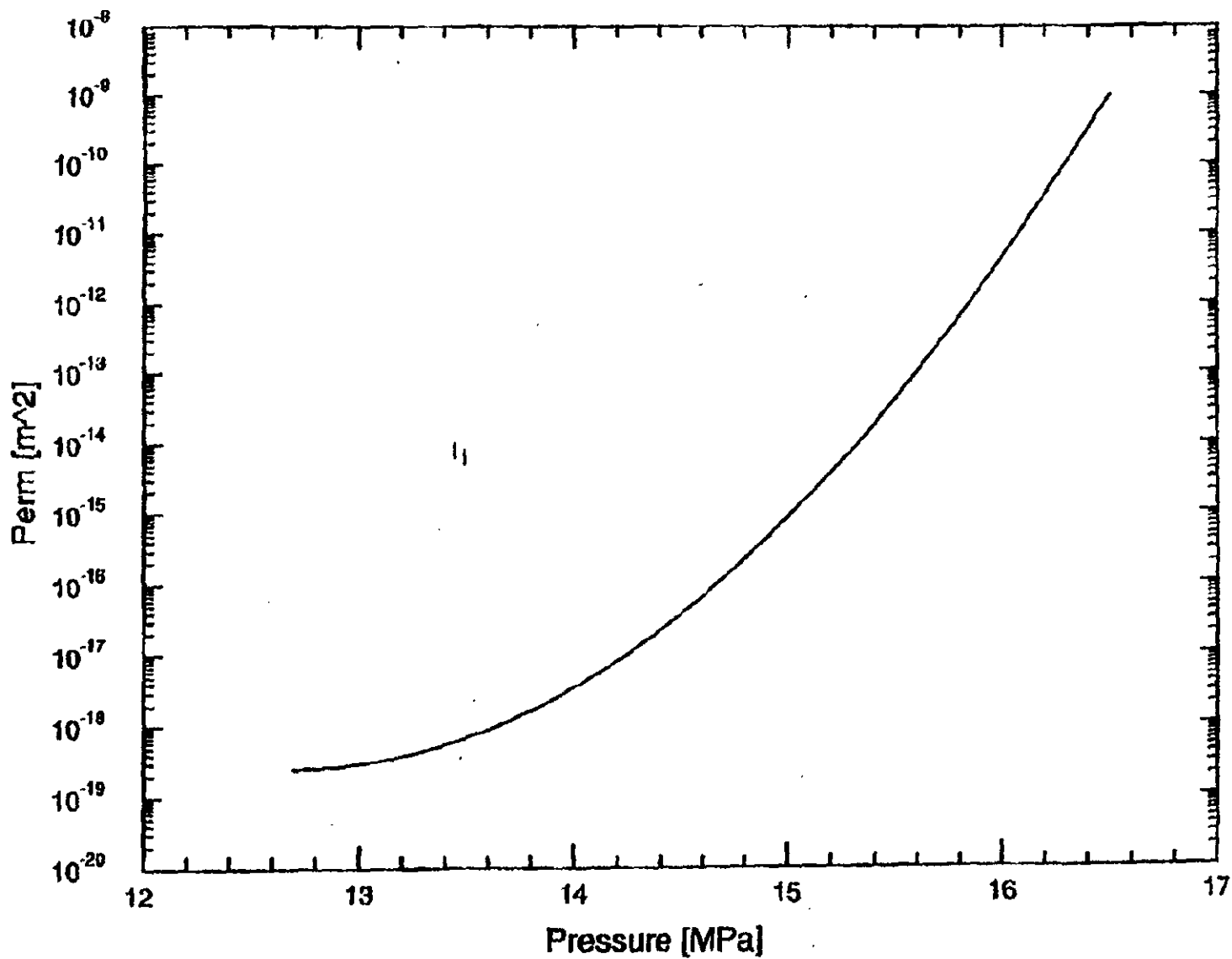


Figure 4: Permeability in Marker Bed A+B with Fracturing

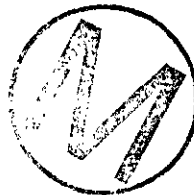


Comparison of Effects of Brine Pocket Size

**Daniel M. Stoelzel, Palmer Vaughn
Sandia National Laboratories, org 6848, 6849**

**Darien G. O'Brien, PE
Solutions Engineering**

July 19, 1996



BACKGROUND

The existence and size of a Castile Brine Pocket below the WIPP repository is uncertain. Brine pockets have been found in the northern Delaware Basin but there is little information on their size. The producibility of brine from these pockets is believed to be related to the interconnectedness of a fracture system. Analysis of WIPP-12 data have led to estimates for the areal extent of several hundred meters (drainage radius as small as 230 m – dimension smaller than the WIPP waste-area footprint) to several kilometers (drainage radius as large as 19,000 m – dimension larger than the land withdrawal boundary). DOE does not consider the 19 km radius brine pocket a realistic size, never the less it is included for comparison to other sizes. Because of the interconnectedness of the fracture system, the thickness of the brine pocket has been estimated to be from 7 m to 24 m with a maximum possible of 133.6 m (recent estimate based upon the total thickness of the Castile formation and NOT considered in the 1996 CCA calculations).

Each time a well penetrates the brine pocket, the pressure in the surrounding drainage area depletes. This pressure depletion will extend to those portions of the brine pocket which are interconnected. Passive Institutional Controls shield a region of the Castile from exploratory drilling directly under the waste panels. The 1996 CCA calculations assume that the Castile Brine Pocket under the waste panels is weakly interconnected hydraulically (with vertical and areal extents similar to the lower estimates from WIPP-12, i.e. total brine volume between 32,000 and 160,000 m³ [Larson & Freeze, 1996]), and is not much affected by penetrations occurring outside the waste-area footprint. Therefore, the pressure underneath the waste panels in the brine pocket is assumed to not deplete until penetrated by a borehole drilled within the panel area. If the brine pocket has an extensive fracture system (and hence is strongly interconnected), the area beneath the waste panels can be depleted by penetrations outside the waste-area footprint.

This study looks at the consequences of assuming that the brine pocket is hydraulically interconnected such that borehole penetration depletion impacts are felt throughout a larger drainage area. The total brine volume which migrates from the Castile Brine Pocket to the Culebra aquifer with depletion impacts (large drainage area) is compared against the brine volume migration without depletion (small drainage area).



THEORETICAL CONSIDERATIONS

For the 1996 CCA calculations, an abnormally pressured Castile Brine Pocket is assumed (i.e. the brine pocket pressure exceeds the anticipated hydrostatic pressure). The brine pocket is assumed to be bounded (i.e. of limited thickness and areal extent) rather than infinite acting (such as the Culebra aquifer). Consistent with DOE regulatory criteria regarding the rate of future drilling activity, it is assumed that 47 boreholes will be drilled per square kilometer over the next 10,000 years (or 0.47/100 yrs/km²). Each penetration of the abnormally pressured brine pocket will result in flows according to the following time horizons:

1) **Time of intrusion to 72 hours** - brine flows from the brine pocket, past the Culebra all the way to the surface during active drilling through an open borehole (assuming steady-state flow conditions). A computation to determine the length of time during which steady-state is valid (i.e. infinite acting period when the pressure sink caused by flow into the borehole has reached the extent of the drainage area) as computed by the following [Lee, 1982]:

$$t < \frac{\phi \mu c_t A t_{DA}}{k} \quad \text{[Equation 1]}$$

where:

- t = Time (for a bounded cylindrical system is infinite acting) (sec)
- ϕ = Porosity (fraction)
- μ = Viscosity (Pa-sec)
- c_t = Total compressibility (Pa⁻¹)
- A = Drainage area (defined as the land withdrawal boundary area/avg. no. of boreholes/200 years where 19.5 boreholes is taken as the average in 200 years) (m²)
- t_{DA} = Dimensionless time (which for a bounded cylindrical system = 0.10, [Lee, 1982])
- k = Brine pocket permeability (m²)

The solution to Equation 1 is approximately 7 hours. Although the steady-state flow assumption is valid only within 7 hours after penetration, a flow period of 72 hours was used. This is consistent with the 1996 CCA blowout time period to obtain direct brine releases from the WIPP repository. For the purposes of this investigation, pressure depletion during the 72 hour open flow period was not taken into account.



During the 72 hour flow period, flowrate is computed from the following (see nomenclature section for definition of variables):

$$Q_{bp} = \left\{ \frac{k_{bp} h_{bp}}{\mu \left[\ln \left(\frac{r_{ew}}{r_w} \right) - 0.5 \right]} \right\} (P_{bp} - P_{atm} - \rho g L_{surface}) \quad \text{[Equation 2]}$$

2) 72 hours to 200 years - no brine flows from the brine pocket since the 1996 CCA calculations assume a 200 year time period immediately following intrusion during which the borehole is plugged at the Rustler and Castile formations.

3) From 200 years to 1200 years - cement plugs are no longer active. Flow occurs between the Castile Brine Pocket and the Culebra aquifer via "silty sand" abandoned boreholes with median permeabilities of $3.16E-13 \text{ m}^2$.

4) 1200 years to 10000 years - median abandoned borehole permeabilities are reduced one order of magnitude ($3.16E-14 \text{ m}^2$) due to salt creep.



Abandoned Borehole Connection Between Castile Brine Pocket and Culebra Aquifer

Consider the flow rate necessary to achieve flow from the Castile Brine Pocket to the Culebra Aquifer through an abandoned borehole as depicted in Figure 1:

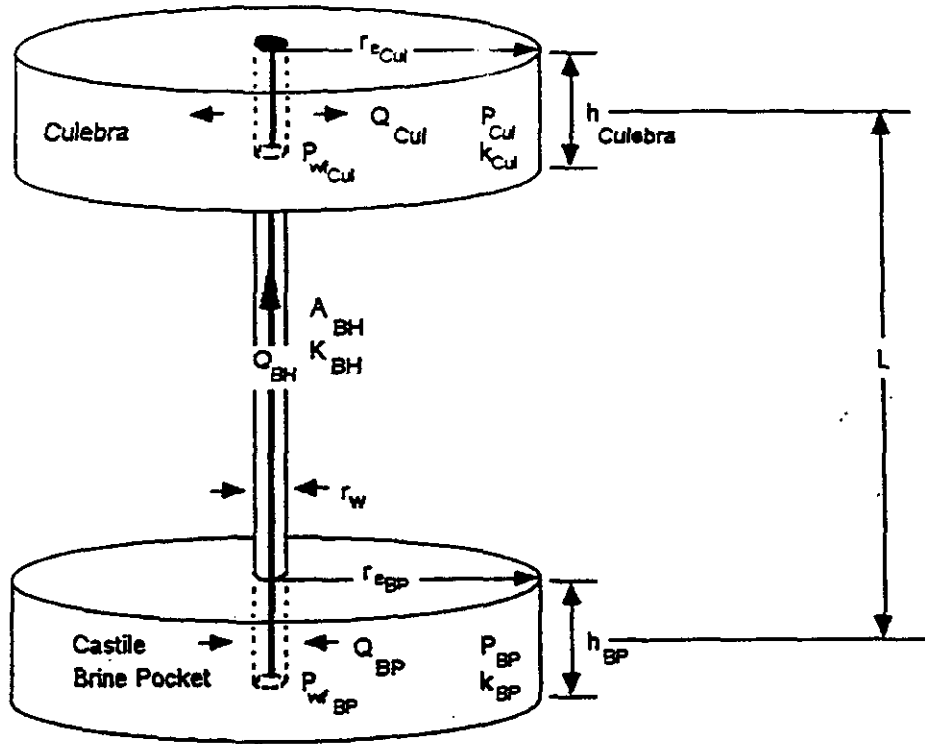


Figure 1: Representation of assumed flow path for Castile Brine Pocket to Culebra Aquifer



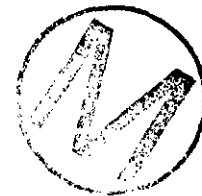
NOMENCLATURE

Define the following variables by:

- Q = Flowrate (m^3/sec)
- k = Permeability (m^2)
- h = Thickness (m)
- μ = Brine viscosity (Pa-sec)
- ρ = Brine density (kg/m^3)
- g = Acceleration due to gravity (m/sec^2)
- L = Borehole length (m)
- r = Radius (m)
- A = Cross sectional area (m^2)
- P = Pressure (Pa)
- \bar{P} = Average pressure between r_e and r_w (Pa)
- c = Compressibility (Pa^{-1})
- ϕ = Porosity (fraction)
- V = Bulk volume (m^3)
- ΔN = Brine volume produced between time 1 and 2 (m^3)

Define the following subscripts by:

- cul = Culebra
- bh = Borehole
- bp = Brine pocket
- e = External drainage per borehole (brine pocket area divided by number of boreholes)
- w = Wellbore
- wf = Abandoned wellbore flowing
- atm = Atmospheric
- b = Rock bulk
- f = Pore volume
- br = Brine
- t = Total
- R = Castile Brine Pocket or Culebra Aquifer
- 1,2 = Time 1, time 2



Refer to Figure 1, assuming steady-state flow is positive between the Castile Brine Pocket and the Culebra Aquifer, the following Darcy Law equations are used to obtain the flowrates out of the brine pocket (Q_{bp}), through the borehole (Q_{bh}) and into the aquifer (Q_{cul}), based upon the pressures, rock and fluid properties and brine pocket/abandoned borehole/aquifer geometries:

$$Q_{cul} = \left\{ \frac{k_{cul} h_{cul}}{\mu \left[\ln \left(\frac{r_{cul}}{r_w} \right) - 0.5 \right]} \right\} (P_{wf_{cul}} - P_{cul}) \quad \text{[Equation 3]}$$



$$Q_{bh} = \left[\frac{k_{bh} A_{bh} (P_{wf_{bh}} - P_{wf_{cul}} - \rho g L)}{\mu L} \right] \quad \text{[Equation 4]}$$

$$Q_{bp} = \left\{ \frac{k_{bp} h_{bp}}{\mu \left[\ln \left(\frac{r_{cul}}{r_w} \right) - 0.5 \right]} \right\} (P_{bp} - P_{wf_w}) \quad \text{[Equation 5]}$$

The flowrates through each of these systems are assumed to be equal (i.e. no fluid leaves the system), therefore:

$$Q_{bp} = Q_{bh} = Q_{cul} \quad \text{[Equation 6]}$$

This results in four equations (Equations 3-6) and two unknowns ($P_{wf_{bp}}$ and $P_{wf_{cul}}$) which can be algebraically solved for Q_{bp} as follows:

$$Q_{bp} = \frac{\left\{ \frac{k_{bp} h_{bp}}{\mu \left[\ln \left(\frac{r_{cul}}{r_w} \right) - 0.5 \right]} \right\} (P_{bp} - \rho g L - P_{cul})}{1 + \left\{ \frac{k_{bp} h_{bp}}{\mu \left[\ln \left(\frac{r_{cul}}{r_w} \right) - 0.5 \right]} \right\} \left[\frac{\mu \left[\ln \left(\frac{r_{cul}}{r_w} \right) - 0.5 \right]}{k_{cul} h_{cul}} + \frac{\mu L}{k_{bh} A_{bh}} \right]} \quad \text{[Equation 7]}$$

Equation 7 is the steady-state solution for flow through the brine pocket/abandoned borehole/aquifer system. To account for bounded brine pocket/aquifer sizes, pressure drawdown can be estimated by redefining the brine pocket and aquifer pressures over a series of discrete time intervals by the following:

The pore volume compressibility (c_f) as a function of rock bulk compressibility (c_b) may be defined by:

$$c_f = \frac{c_b}{\phi} \quad \text{[Equation 8]}$$

The total compressibility (c_t) is the sum of the brine compressibility (c_{br}) and pore volume compressibility (c_f) as follows:

$$c_t = c_{br} + c_f \quad \text{[Equation 9]}$$

The bulk volume of the bounded brine pocket is a function of the volume of brine removed, average pressure drop, compressibility and porosity as follows:

$$V_R = A_R h = \frac{\Delta N_{1,2}}{(\bar{P}_1 - \bar{P}_2) c_t \phi} \quad \text{[Equation 10]}$$

Equation 10 can be used to solve for the average pressure at the end of a given time interval by:

$$\bar{P}_2 = \bar{P}_1 - \frac{\Delta N_{1,2}}{V_R c_t \phi} \quad \text{[Equation 11]}$$



METHODOLOGY AND RESULTS

Since the size of the brine pocket is unknown, comparisons were made for various areal size and thickness as shown in the following table (consistent with interpreted results from WIPP-12 data [Larson & Freeze, 1996]):

Table 1 - Constant Brine Volumes by Varying Thickness and Areal Extent

Thickness (m)	Areal Extent 1 (m ²)	Areal Extent 2 (m ²)	Areal Extent 3 (m ²)
133.6	6.0E+07	3.0E+06	3.0E+04
66.8	12.0E+07	6.0E+06	6.0E+04
24.0	33.4E+07	16.7E+06	16.7E+04

For the Culebra aquifer, the areal extent was assumed to be 100 times the LWB for all cases (4144 km²). All other properties were median values obtained from the 1996

CCA database. The combination of three thicknesses and three areas for the Castile Brine Pocket resulted in 9 cases for comparison. Initial brine pocket pressure was assumed to be 12.7 E+07 Pa for all cases.

Table 2 shows an example spreadsheet calculation assuming an area of 6.0 E+07 m² and 133.6 m brine pocket thickness.

Table 2 - Example Spreadsheet Calculation

BP area	6.00E+07 m ²
Cul area	4.14E+08 m ²
Por (int)	850000 Pa
U	1.80E-03 P=α
rCul	7.7 m
L	641.5 m
Integ L	708.5 m
hBP	133.6 m
Por (int)	1.27E+07 Pa
αBH	3.18E-13 m ²
αCUL	2.18E-14 m ²
rw	0.1886 m
Area BH	0.0780822 m ²
αBP	1.11E-12 m ²
rw	230 μm=0
g	9.8
rw'g'1 open	8.5E+6 Pa
rw'g'1 open	11.2E+6 Pa
h'year	3.18E+07
press BP	0.008
press Cul	0.151
Cl BP	1.00E-10 1/Pa
Cl Cul	1.00E-10 1/Pa
Cl BP	1.23E-06 1/Pa
Cl Cul	6.02E-10 1/Pa
Clms	1.00E-09 1/Pa
Cl BP	1.35E-06 1/Pa
Cl Cul	1.88E-09 1/Pa
Brine Pocket bulk vol =	8.0E+8 m ³
Castile bulk vol =	31.9E+8 m ³
Open BH Cl	2.58E+05 seconds
No. open BH=Cl	2.82E+01
rw BP	822.95508
Press	101320 Pa
Clf rate	0.47 bh/m ² /100years

Time years	Num BH in BP	Number of sand BH of creep	Number of creep BH	BP press Pa	Cul Press Pa	BP radius per bh BH m	Cul radius per well m	Const	Clp open BH per well m ² /a	delta flow open m ³ /o
200.0	56.40	0.0	0.0	12.7E+6	850.0E+3	4.3702E+13	4.37E+13	3.58E-08	0.020485974	149.8E+3
400.0	112.80	28.2	0.0	12.5E+6	850.0E+3	822.95508	4.37E+13	1.45E-08	0.017955988	131.2E+3
600.0	169.20	84.9	0.0	12.4E+6	851.3E+3	473.133342	4.37E+13	1.58E-08	0.018578228	113.9E+3
800.0	225.60	141.0	0.0	12.2E+6	855.0E+3	388.036704	4.37E+13	1.81E-08	0.013168822	96.3E+3
1,000.0	282.00	197.4	0.0	12.0E+6	860.9E+3	311.047798	4.37E+13	1.96E-08	0.010789845	78.7E+3
1,200.0	338.40	253.8	0.0	11.9E+6	864.5E+3	274.318283	4.37E+13	1.88E-08	0.008417987	61.5E+3
1,400.0	394.80	310.2	0.0	11.7E+6	877.8E+3	248.130288	4.37E+13	1.71E-08	0.006145644	44.9E+3
1,600.0	451.20	366.6	84.8	11.8E+6	888.3E+3	228.248874	478.1333	1.73E-08	0.0038778128	28.1E+3
1,800.0	507.60	388.8	84.8	11.4E+6	906.2E+3	228.248874	478.1333	1.73E-08	0.001891258	13.8E+3
2,000.0	564.00	388.8	141.0	11.3E+6	911.2E+3	228.248874	388.0367	1.73E-08	0.000176823	1.3E+3
2,200.0	620.40	388.8	197.4	11.2E+6	921.7E+3	228.248874	311.0478	1.73E-08	0	0.00E+0
2,400.0	676.80	388.8	253.8	11.1E+6	931.7E+3	228.248874	274.3184	1.73E-08	0	0.00E+0
2,600.0	733.20	388.8	310.2	11.0E+6	941.2E+3	228.248874	248.1303	1.73E-08	0	0.00E+0
2,800.0	789.60	388.8	366.6	10.9E+6	950.3E+3	228.248874	228.2487	1.73E-08	0	0.00E+0
3,000.0	846.00	388.8	423.0	10.8E+6	958.0E+3	228.248874	212.4881	1.73E-08	0	0.00E+0
3,200.0	902.40	388.8	479.4	10.8E+6	967.3E+3	228.248874	199.5889	1.73E-08	0	0.00E+0
3,400.0	958.80	388.8	535.8	10.7E+6	975.2E+3	228.248874	186.7988	1.73E-08	0	0.00E+0
3,600.0	1,015.20	388.8	592.2	10.6E+6	982.8E+3	228.248874	179.5835	1.73E-08	0	0.00E+0
3,800.0	1,071.60	388.8	648.6	10.6E+6	988.7E+3	228.248874	171.588	1.73E-08	0	0.00E+0
4,000.0	1,128.00	388.8	705.0	10.5E+6	994.4E+3	228.248874	164.581	1.73E-08	0	0.00E+0
4,200.0	1,184.40	388.8	761.4	10.5E+6	1.0E+6	228.248874	158.3778	1.73E-08	0	0.00E+0
4,400.0	1,240.80	388.8	817.8	10.4E+6	1.0E+6	228.248874	152.8189	1.73E-08	0	0.00E+0
4,600.0	1,297.20	388.8	874.2	10.3E+6	1.0E+6	228.248874	147.9071	1.73E-08	0	0.00E+0
4,800.0	1,353.60	388.8	930.6	10.3E+6	1.0E+6	228.248874	143.2581	1.73E-08	0	0.00E+0
5,000.0	1,410.00	388.8	987.0	10.3E+6	1.0E+6	228.248874	138.1048	1.73E-08	0	0.00E+0
5,200.0	1,466.40	388.8	1,043.4	10.2E+6	1.0E+6	228.248874	133.288	1.73E-08	0	0.00E+0
5,400.0	1,522.80	388.8	1,099.8	10.2E+6	1.0E+6	228.248874	131.7763	1.73E-08	0	0.00E+0
5,600.0	1,579.20	388.8	1,156.2	10.1E+6	1.0E+6	228.248874	128.524	1.73E-08	0	0.00E+0
5,800.0	1,635.60	388.8	1,212.6	10.1E+6	1.0E+6	228.248874	125.4895	1.73E-08	0	0.00E+0
6,000.0	1,692.00	388.8	1,269.0	10.1E+6	1.0E+6	228.248874	122.6789	1.73E-08	0	0.00E+0
6,200.0	1,748.40	388.8	1,325.4	10.0E+6	1.0E+6	228.248874	120.0403	1.73E-08	0	0.00E+0
6,400.0	1,804.80	388.8	1,381.8	10.0E+6	1.1E+6	228.248874	117.588	1.73E-08	0	0.00E+0
6,600.0	1,861.20	388.8	1,438.2	10.0E+6	1.1E+6	228.248874	115.2388	1.73E-08	0	0.00E+0
6,800.0	1,917.60	388.8	1,494.6	9.9E+6	1.1E+6	228.248874	113.0416	1.73E-08	0	0.00E+0
7,000.0	1,974.00	388.8	1,551.0	9.9E+6	1.1E+6	228.248874	110.9472	1.73E-08	0	0.00E+0
7,200.0	2,030.40	388.8	1,607.4	9.9E+6	1.1E+6	228.248874	109.0031	1.73E-08	0	0.00E+0
7,400.0	2,086.80	388.8	1,663.8	9.9E+6	1.1E+6	228.248874	107.1398	1.73E-08	0	0.00E+0
7,600.0	2,143.20	388.8	1,720.2	9.9E+6	1.1E+6	228.248874	105.3888	1.73E-08	0	0.00E+0
7,800.0	2,199.60	388.8	1,776.6	9.9E+6	1.1E+6	228.248874	103.8028	1.73E-08	0	0.00E+0
8,000.0	2,256.00	388.8	1,833.0	9.9E+6	1.1E+6	228.248874	102.078	1.73E-08	0	0.00E+0
8,200.0	2,312.40	388.8	1,889.4	9.9E+6	1.1E+6	228.248874	100.54	1.73E-08	0	0.00E+0
8,400.0	2,368.80	388.8	1,945.8	9.9E+6	1.1E+6	228.248874	99.07215	1.73E-08	0	0.00E+0
8,600.0	2,425.20	388.8	2,002.2	9.9E+6	1.1E+6	228.248874	97.8888	1.73E-08	0	0.00E+0
8,800.0	2,481.60	388.8	2,058.6	9.9E+6	1.1E+6	228.248874	96.31881	1.73E-08	0	0.00E+0
9,000.0	2,538.00	388.8	2,115.0	9.7E+6	1.1E+6	228.248874	95.02667	1.73E-08	0	0.00E+0
9,200.0	2,594.40	388.8	2,171.4	9.7E+6	1.1E+6	228.248874	93.79444	1.73E-08	0	0.00E+0
9,400.0	2,650.80	388.8	2,227.8	9.7E+6	1.1E+6	228.248874	92.58888	1.73E-08	0	0.00E+0
9,600.0	2,707.20	388.8	2,284.2	9.7E+6	1.1E+6	228.248874	91.45845	1.73E-08	0	0.00E+0
9,800.0	2,763.60	388.8	2,340.6	9.7E+6	1.1E+6	228.248874	90.39108	1.73E-08	0	0.00E+0
10,000.0	2,820.00	388.8	2,397.0	9.7E+6	1.1E+6	228.248874	89.28201	1.73E-08	0	0.00E+0



Figure 2 is a semilog plot comparing the number of borehole penetrations for different brine pocket areal sizes based upon the DOE criterion of 0.47/100 year/km² drilling rate. The same number of penetrations apply to each respective areal size regardless of thickness.

Figure 2

Comparison of Drilling Penetrations to Castile Brine Pocket for Different Areas

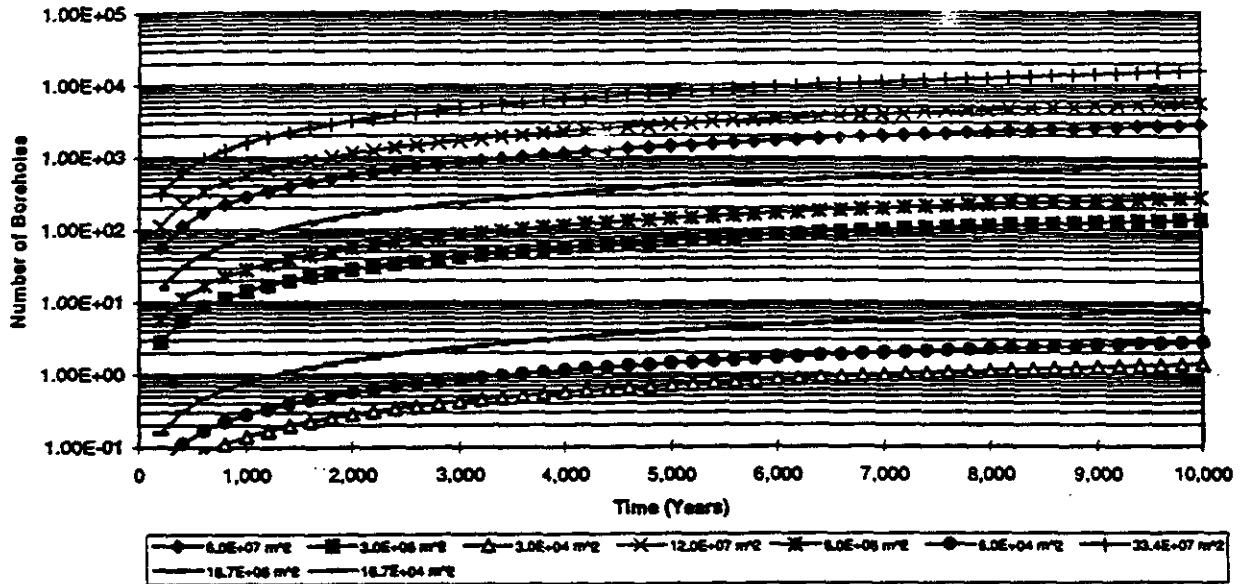
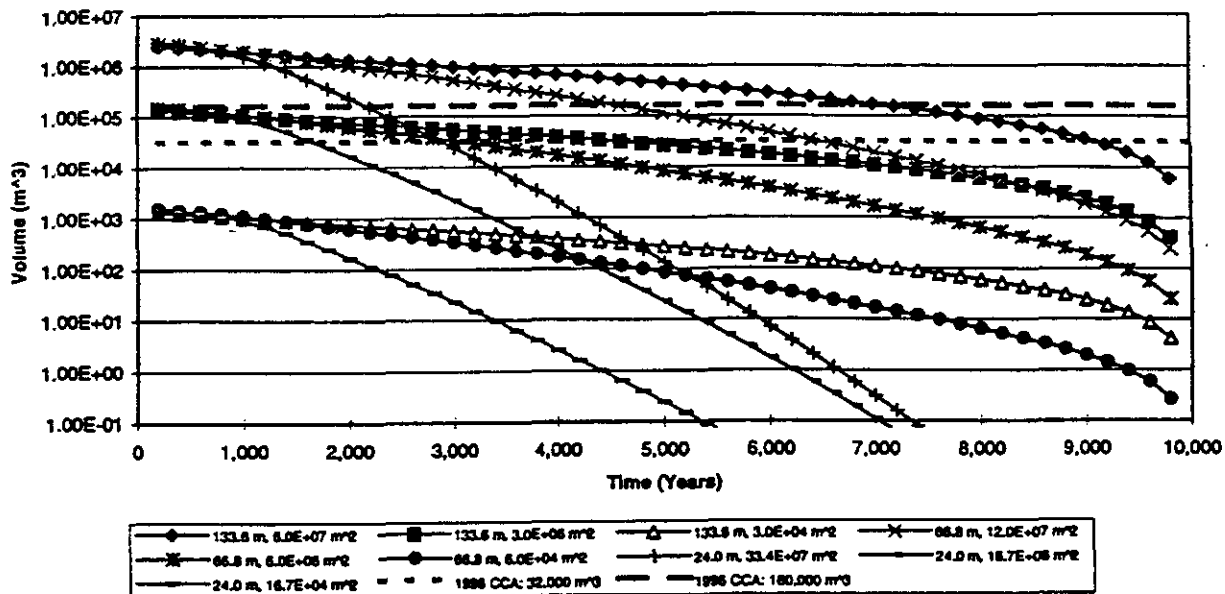


Figure 3 is a semilog plot comparing the amount of Castile brine volume which can be released. This was determined by subtracting the cumulative brine released at a given time from the total cumulative brine released at 10,000 years. The 24 m thickness cases again demonstrate faster depletion than the corresponding 133.6 m thickness cases of equivalent area. For a given thickness, the differences in remaining available flow is caused by differences in the number of depletion boreholes which is a function of the area.

Figure 3

Comparison of Remaining Castile Brine Available for Flow
 (Initial Pbp = 12.7 MPa, 72 hour open flow period)



CONCLUSIONS

The 1996 CCA calculations varied the brine pocket volume from 32,000 m³ to 160,000 m³. From Figure 3, the only cases which show more brine available for flow for an extended period of time (~2000 to ~7000 years) are the maximum area cases. DOE does not consider the 19 km radius brine pocket to be a realistic estimate of the areal extent, rather an artifact of the unreasonably low rock compressibility ($5 \times 10^{-12} \text{ pa}^{-1}$) used for that estimate. In addition, the DOE does not include the depressurization or volume reduction to the brine pocket that would result in numerous borehole penetrations that would statistically "miss" a WIPP panel but penetrate the brine pocket, prior to the first "E1" borehole through a panel. In the CCA calculations for E1 scenarios, the DOE assumes brine pockets of 32,000 m³ to 160,000 m³ pore volume at virgin (undepleted) pressures in determining potential releases to the accessible environment, which bounds the range of consequences associated with penetrating a larger but partially depleted brine pocket.

REFERENCES

[Larson & Freeze, 1996]: Larson, Kurt and Freeze, Geoff, Memorandum of Record, "Castile Brine Reservoir Volume Revision", SWCF-A:WBS1.2.07.1:PDD:NON-SALADO:PKG#19C:Castile Brine Reservoir Volume (WPO #31082), May 27, 1996.

[Lee, 1982]: Lee, John, Well Testing, American Institute of Mining, Metallurgical, and Petroleum Engineers, Inc. ISBN 0-89520-317-0, 1982, (Example 1.3), p. 8, (Table 1-2), p. 9.





The University of New Mexico

New Mexico Engineering Research Institute
Albuquerque, NM 87131-1376
USA

Date: July 19, 1996

To: Margaret Chu, MS-1335 (6801)

J.W. Berglund, Jonathan Myers, Larry R. Lenke
From: J. W. Berglund 6849, NMERI; J. Myers, IT Corp; L.R. Lenke, NMERI

Subject: Estimate of the Tensile Strength of Degraded Waste for use in Solids Blowout

A value of 1 psi (6895 Pa) was chosen to represent the tensile strength of decomposed waste for the purpose of computing blowout spall releases resulting from a drillbit intrusion into a pressurized waste panel. Such spall releases occur only if the gas pressure exceeds the hydrostatic drilling mud pressure of approximately 8 MPa. A chemical reaction between the waste and brine from the surroundings is necessary to generate the gas to raise the waste pore pressure to these levels. Without brine inflow, little gas will be generated and waste decomposition will be negligible. Thus the phenomenon of blowout spall requires both brine inflow and waste decomposition.

The future state of decomposed waste is both time dependent and unknowable. Therefore a decomposed state consisting of graded granular materials is assumed. This is consistent with the granular nature of decomposed geologic materials and corresponds to an end state of the decomposition process. Such materials lack significant composite strength from the interleaving of components and is the state found to be most troublesome in oil production where sand is produced from poorly consolidated sand layers. The value of 1 psi chosen for cementation strength for the decomposed waste can be reasonably expected to be conservative, i.e. lower than those data values found for many weak materials that are naturally occurring or that have been manufactured. Data to support this value can be found in the literature for the strengths of soils, laboratory produced mixtures of salt and clay, and mixtures of various materials with MgO; the latter added as a backfill material to the waste. A discussion of these data sources follows.

Soil Data

Tensile strengths for several compacted, cohesive soils e.g. Vicksburg buckshot clay (CH), Vicksburg lean clay (CL), and a sandy clay mixture from De Gray dam (SC) were measured using hollow cylinder tests and indirect tensile tests in Al-Hussaini (1981). The samples were prepared to optimum water content compacted and tested. Results for the hollow cylinder tests are shown in Table 1. All exceed 1 psi by factors of approximately 3 to 8 times. Similar results were obtained from the indirect tensile tests.



Table 1 Hollow Cylinder Tests

Material type	Tensile Strength (psi)
CL-1	2.95
CL-2	3.90
CL-3	3.93
CH-1	7.93
CH-2	7.41
CH-3	7.99
SC-1	5.90
SC-2	5.38
SC-3	4.49
CH-4	6.46
CH-5	6.12
CH-6	6.52



Direct tensile tests on simulated waste materials were also conducted by Berglund and Lenke, 1995, p13-14. Various mixtures of partially saturated silica sand and kaolin clay were used to represent the waste. The clay represented a natural material that was chosen to be a close surrogate to partially decomposed cellulose and plastics. The sand represented the particulate structure expected of magnetite or other products of the iron corrosion reaction. The mixture was 85% sand and 15% clay, a ratio similar to the ratio of decomposition products anticipated for some waste conditions. The tensile strength measured in these experiments was 2.9 ± 1.4 psi. A second indirect method of measuring tensile strength in the Berglund, Lenke study implied an even higher tensile strength value of 4.3 ± 1 psi.

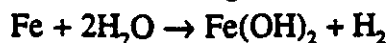
The tensile strength of the above materials (Al-Hussaini 1981, Berglund and Lenke 1995) occurred in the absence of any additional cementation process which would tend to increase these measured tensile strengths.

Salt Mixture Data

Some brine is expected to exist within the waste panels after closure of the facility. The most likely source is brine of Permian age that was trapped in the Salado formation at the time of evaporite deposition. Limited brine occurrences in the WIPP underground have been extensively sampled and analyzed, and the composition of Salado brine is well understood. These brines contain approximately 374 grams of dissolved constituents per liter and are in chemical equilibrium with halite (NaCl) anhydrite (CaSO₄), and magnesite (MgCO₃).

The removal of even a small amount of water from this brine by evaporation or chemical reaction will result in the precipitation of salts which will act as a cementation agent. One such chemical reaction that is anticipated to occur is the anoxic corrosion of iron and ferrous alloys, which constitute a significant percentage of the waste inventory in the form of steel drums and boxes, contaminated tools and sheet metal, etc.

The reaction of brine with metal will consume H₂O and generate hydrogen and some corrosion product. A typical anoxic reaction might be



Consumption of H₂O by corrosion reactions will cause the mass of dissolved solids in the brine to precipitate as a series of evaporite minerals in close proximity to the surface of the

corroding metals forming encrustations which tend to cement the waste. Simulation of the removal of H₂O from one kg of Salado brine using the EQ6 code (Wolery T.J., and S.A. Daveler, 1992) yielded 534 grams of precipitates (anhydrite, bischofite, carnallite, halite, kieserite, and magnesite). The mass is greater than the mass of dissolved solids because of the hydrous nature of some of the precipitates.

Evidence for this process in the WIPP underground could be seen at the close of heated brine inflow experiments performed by SNL a number of years ago. In these experiments, a metal canister containing an electrical heater was placed in a vertical hole excavated in the floor of a room in the northern experimental area. The top of the hole was sealed, and anhydrous nitrogen was circulated within the annulus between the canister and the hole. Small amounts of brine flowed toward the hole in response to the pressure and temperature gradients surrounding the heated hole, and evaporated as it approached the canister. The nitrogen acted as a carrier gas for water vapor and was allowed to exit the hole where it flowed into an apparatus where the water vapor was extracted and quantified.

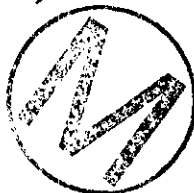
It was found at the close of the experiment that the canister has become firmly cemented in the hole by the precipitation of salts from the evaporating brine within the annulus. A work-over rig had to be employed to extract the canister from the hole. The removal of water from brine by any process, be it evaporation or corrosion reactions, will produce the same cementation effect by the precipitation of minerals at the site of water removal. This cementation will act to increase the strength of the waste.

A number of strength tests were done for consolidated crushed WIPP salt and mixtures of WIPP salt and bentonite (70 and 30% respectively) (Finley, 1996). Finley's memorandum presents estimates of tensile strengths of clay/salt mixtures based on experimental observations of unconfined compressive strengths and the extended Griffith criterion for tensile failure (Jaeger and Cook, 1976). These estimates are for 30/70 percent bentonite/salt mixtures at fractional densities of 0.83 to 0.88. Finley estimates tensile strengths between 10 and 100 psi.

The WIPP waste stream upon creep closure and subsequent brine saturation will consist of approximately 1350 kg of waste solids (assumed average solid density of the waste was taken as 2700 kg/m³) and 188 kg of precipitated salt (based on dissolved salt solids of 374 gram/liter cited above) per cubic meter of repository. These numbers are based on a typical closure porosity of 0.5 (final room height of 1.2 m). The gravimetric ratio of salt precipitate to solid waste for these conditions is 0.14. This is a factor of 5 less than the ratio cited by Finley. Using this factor, it is not unreasonable to expect tensile strengths between 2 and 20 psi.

Effects of MgO on Strength

An additional process affecting the strength of the waste/backfill composite material is the chemical interactions that will occur between Salado brine and the MgO backfill. These interactions were simulated using the EQ3/6 code (Wolery, 1992; and Wolery T.J., and Daveler, 1992) with the Pitzer activity coefficient option and Harvie-Moller-Weare database. Five moles of MgO were reacted with one kilogram of Salado brine in a series of small steps. The dissolution of the five moles (202 grams) of MgO into the brine resulted in the precipitation of a total of 507 grams of minerals and the incorporation of 20 percent of the original kg of brine as water of hydration within the precipitates. These precipitates include Mg-oxychloride (63% by mass) and brucite (31% by mass), with minor amounts of anhydrite, halite, and magnesite. Similar results were found by Wang, 1996.



The two dominant precipitates (Mg-oxychloride and brucite) are the key phases in Sorel cement. In fact, Sorel cement is commercially prepared by mixing a magnesium-chloride brine (quite similar to Salado brine) with MgO. Sorel cement is known to have uniaxial compressive strengths in the range of 7,000 to 10,000 psi (Sax and Lewis, 1987). This range is equivalent to tensile strengths of from 490 to 700 psi (Dunham C.W., 1966). Thus the use of an MgO backfill will result in the cementation and strengthening of the waste/backfill composite material as long as sufficient brine is available for the chemical reactions to occur.

Conclusions

While tests to actually measure the binding forces between particles of simulated waste have not been performed, there are data available from several independent sources that suggest that the selection of 1 psi is well below the actual value of tensile strength that can be reasonably expected for decomposed waste. The tensile data presented for several soils without chemically generated salt precipitates exceed 1 psi by factors generally greater than 3. Estimated tensile strengths of consolidated halite-bentonite mixtures exceed 1 psi by factors of ten or more. The role of precipitated salts from anoxic reactions of brine with waste metals is expected to be similar though perhaps not as intense. MgO is added to the waste as a backfill material in large volumes. The reaction products of MgO plus brine are the principal components of Sorel cement which attains high compressive strengths and predicted tensile strengths of 490 to 700 psi.

References

Al-Hussaini, M. (1981), *Tensile Properties of Compacted Soils*, Laboratory Shear Strength of Soil, ASTM STP 740, R. N. Yong and F. C. Townsend, Eds., American Society for Testing Materials, pp.207-225.

Berglund, J.W., and Lenke, L.R., 1995, *One Dimensional Experiments of Gas Induced Spall*, NMERI 1995/3, prepared for Sandia National Laboratories, New Mexico Engineering Research Institute, University of New Mexico, Albuquerque, NM, February 1995 WPO# 27589.

Dunham C.W., 1966, *The Theory and Practice of Reinforced Concrete*, McGraw-Hill, New York, p 36.

Finley, R.E. May 3, 1996 Memorandum to D.R. Anderson and M.S.Y. Chu, Subject: Tensile Strength of Consolidated Crushed Salt

Jaeger, J.C. and N.G.W. Cook, 1979, *Fundamentals of Rock Mechanics*, 3rd Edition, Chapman and Hall, London

Sax, N. I, and R. J. Lewis, 1987, *Hawleys Condensed Chemical Dictionary*, Eleventh Edition, Van Nostrand Reinhold, New York.

Wang Y., 1996, Memorandum to Malcolm Siegel, March 18, 1996, Subject: Define Chemical Conditions for FMT Actinide Solubility Calculations SWCF-A, WBS 1.1.09.1.1(BC);QA

Wolery T.J., 1992, EQ3NR, *A Computer Program for Geochemical Aqueous Speciation-Solubility Calculations: Theoretical Manual, Users Guide, and Related Documentation* (Version 7.0). Lawrence Livermore Laboratory, Livermore California.



Wolery T.J., and S.A. Daveler, 1992, EQ6, *A Computer Program for Reaction Path Modeling of Aqueous Geochemical Systems: Theoretical Manual, Users Guide, and Related Documentation (Version 7.0)*. Lawrence Livermore Laboratory, Livermore California.

cc:

MS 1330 SWCF-A:1.1.01.2.7:DRM:QA:Waste Strength, TD



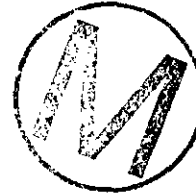
Sandia National Laboratories

Albuquerque, New Mexico 87185-1341

date: August 20, 1996

to: Distribution

from: ¹¹ D. W. Hicks Yifeng Wang D. W. Hicks
David Bennett, Yifeng Wang, and Tim Hicks



subject: An Evaluation of Heat Generation Processes for the WIPP

1.0 Introduction

Nuclear criticality, exothermic reactions, and radioactive decay are possible sources of heat in the WIPP repository. Nuclear criticality has been eliminated from performance assessment calculations on the basis of low probability (see SNL Summary Memo of Record RNT-1). This memo discusses possible heat generating processes at the WIPP and the potential magnitude of the temperature increases they might induce. Heat from exothermic reactions is discussed in Section 2 and heat from radioactive decay is discussed in Section 3.

Conclusions are provided in Section 4. In summary, soon after disposal concrete hydration in the panel closures and shaft seals will give rise to temperature increases lasting a few decades. Heat from radioactive decay will generate a maximum temperature increase of less than 2°C above the ambient temperature (about 27°C) within 100 years after disposal. A number of potential exothermic reactions other than concrete hydration have been identified. These reactions are brine limited and will cause only minor perturbations to the temperature distribution within the disposal system. The maximum calculated rate of brine inflow to a waste disposal panel, and thus, the maximum exothermic reaction rates, occur for the S2 scenario involving an E1 drilling event at 350 years after disposal. By the time such a drilling event takes place heat generation from concrete seal hydration and radioactive decay will have decreased substantially, and the temperatures in the disposal rooms will have reduced to close to initial values. Note that active institutional controls are expected to prevent drilling within the controlled area for 100 years after disposal. Thus, exothermic reactions following a drilling intrusion into a waste disposal panel will be the only potentially significant heat generating processes at the time of a drilling intrusion.

The maximum temperature that could be achieved in the panel following a drilling intrusion at 350 years occurs as a result of aluminum corrosion; this reaction could result in a maximum temperature increase of about 6°C two years after the drilling event. This predicted value of temperature increase is based on several conservative assumptions. For example, it is assumed that no aluminum corrosion has occurred prior to the drilling event and that all the brine introduced to the waste panel is available for aluminum corrosion. In reality some aluminum corrosion is likely to have occurred prior to the drilling event, reducing the volume of aluminum available for the reaction, and other reactions with lower reaction enthalpies (such as backfill hydration) or lower reaction rates (such as microbial degradation) will compete with aluminum corrosion to consume brine resulting in a smaller temperature increase. Based on similar conservative assumptions, backfill hydration could result in a maximum temperature increase of less than 5°C. These maximum heat generation rates resulting from aluminum corrosion and backfill hydration could not occur simultaneously because they are limited by brine availability. Thus, the temperature rise of 6°C represents the maximum that could occur as a result of any combination of exothermic reactions occurring simultaneously.



2.0 Heat From Exothermic Reactions

Exothermic reactions in the repository will liberate heat resulting in elevated temperatures. The magnitude and duration of this temperature increase will depend on the amount and rate of energy release, the geometry of the heat source, the thermal conductivities of the surrounding rocks, and any influence of groundwater or brine flow on heat transport.

In the WIPP a range of different types of reactions will occur, including corrosion, microbial degradation, waste dissolution, and concrete and backfill hydration, and these will liberate different amounts of heat at different times. The amount of heat liberated by the different reactions will depend on the extent of reaction that occurs (for example, how much gas generation or concrete hydration takes place), and the enthalpy of the reactions. The former will depend on the inventory of materials emplaced in the WIPP, and the subsequent chemical evolution of the repository system. The latter can be assessed by considering typical enthalpies for the reaction types of interest.

Enthalpies of reaction, $\Delta_r H^\circ$, for example reactions representing processes that may take place in the repository are given in Table 1 (from SNL Summary Memo of Record GG-7, SP-7). The reactions shown are based on the chemical conditions expected in the WIPP. Note that negative values for $\Delta_r H^\circ$ indicate that the reactions liberate heat as they progress from left to right.

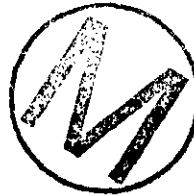


Table 1. Enthalpies of reaction, $\Delta_r H^\circ$, for the WIPP

Reaction	Example Stoichiometry and Standard Enthalpies of Formation, $\Delta_f H^\circ$ (kJ/mol)	Reaction Enthalpy $\Delta_r H^\circ$ (kJ/mol)	Data Source
Backfill hydration	$\Delta_r H^\circ$ $\text{MgO}_{(s)} + \text{H}_2\text{O}_{(l)} = \text{Mg(OH)}_{2(s)}$ -601.7 -285.8 -925.5	-38	Krauskopf, 1982, 561
Backfill carbonation	$\Delta_r H^\circ$ $\text{Mg(OH)}_2 + \text{CO}_2(g) = \text{MgCO}_3 + \text{H}_2\text{O}$ -925.4 -393.1 -1110.3 -285.8	-77	Drever, 1982, 351-256
Microbial degradation	$\Delta_r H^\circ$ $\text{C}_6\text{H}_{10}\text{O}_5 + \text{H}_2\text{O} = 3\text{CH}_4 + 3\text{CO}_2$ -805.5 -285.8 3 x (-74.4) 3 x (-393.5)	-312	Lide, 1994, 5-16 to 5-37
Aluminum Corrosion	$\Delta_r H^\circ$ $\text{Al} + 3\text{H}_2\text{O} = \text{Al(OH)}_3 + 1.5\text{H}_2$ 0 3x(-285.8) 1291.9 0	-434	Drever, 1982, 351-256
Anoxic corrosion of steel	$\Delta_r H^\circ$ $\text{Fe}_{(s)} + 2\text{H}_2\text{O}_{(l)} = \text{Fe(OH)}_{2(s)} + \text{H}_{2(g)}$ 0 2 x (-285.8) -569.0 0	+2.7	Wagman et al., 1982, Table 41
Waste dissolution	$\Delta_r H^\circ$ $\text{UO}_{2(s,cr)} + 2\text{H}_2\text{O}_{(l)} = \text{U(OH)}_{4(aq)}$ -1085.0 2 x (-285.8) -1655.8	+0.9	Grenthe et al., 1992, Table III-1
Concrete hydration	$\Delta_r H^\circ$ $\text{CaO}_{(s)} + \text{H}_2\text{O}_{(l)} = \text{Ca(OH)}_{2(s)}$ -635.1 -285.8 -986.1	-65.2	Wagman et al., 1982, 2-26

Even though there is uncertainty surrounding the extent of reactions that will occur, the reaction enthalpies indicate that the thermal effects of anoxic corrosion of steel and the waste dissolution reaction will be endothermic and will be of low consequence to the performance of the disposal system. However, the other reactions shown in Table 1 have the potential to evolve significant amounts of heat. The potential effects of these processes on the temperature within the disposal system are discussed below.

2.1 Backfill Hydration

Potential temperature increases in the repository as a result of exothermic backfill hydration reactions have been evaluated by Wang (1996, attachment to this memo). In his analysis, Wang (1996) made the following assumptions:

- The reaction will proceed rapidly so that the rate of heat generation will be



controlled by brine availability.

- All brine entering a waste disposal panel will contact and react with the backfill in the panel uniformly.
- All of the emplaced backfill will undergo hydration.

The maximum calculated rate of brine inflow into a panel (about 200 m³/year) occurs for the S2 scenario involving an E1 drilling event at 350 years after disposal. The molar density of water is 5.56x10⁴ moles/m³, and thus, the reaction rate of backfill hydration in the panel will be 1.1x10⁷ moles/year. Based on the reaction enthalpy shown in Table 1, backfill hydration will generate a thermal load of about 13 kW. There will be about 2x10⁸ moles MgO emplaced per panel and thus the reaction could continue for about 20 years if sufficient brine was available.

Wang (1996) estimated the maximum temperature that could be generated by backfill hydration within a panel. Assuming heat loss will occur by conduction through the salt forming the roof and floor of the panel and that heat losses through the side walls are negligible, Wang (1996) calculated that the maximum temperature rise in a panel, as a consequence of backfill hydration following a borehole intrusion and subsequent brine inflow, would be about 4.5°C.

2.2 Backfill Carbonation

Wang (1996) also estimated the potential temperature rise that could occur as a result of backfill carbonation. Wang (1996) assumed that the reaction will be limited by microbial CO₂ production; the maximum rate of CO₂ production is 2.9x10⁵ moles/year. Based on the reaction enthalpy shown in Table 1, backfill carbonation will generate a thermal load of about 0.7 kW. About 3.6x10⁷ moles CO₂ could be produced in a single panel (see Wang, 1996) and thus the reaction could continue for about 125 years. Wang (1996) estimated the maximum temperature that could be generated by backfill carbonation within a panel to be about 0.6°C.

2.3 Microbial Degradation

Wang (1996) estimated the maximum reaction rate for microbial degradation in a panel to be about 1x10⁵ moles/year and the inventory to be about 1.2x10⁷ moles C₆H₁₀O₅ per panel. Thus, the reaction could continue for about 120 years. Based on the reaction enthalpy shown in Table 1, microbial degradation will generate a thermal load of about 1 kW. Wang (1996) estimated the maximum temperature that could be generated by microbial degradation within a panel to be about 0.8°C.



2.4 Aluminum Corrosion

Wang (1996) determined that the rate of corrosion of aluminum will be controlled by brine availability. From Table 1, the reaction rate of aluminum corrosion in the panel will be about 0.4×10^7 moles/year, assuming a brine inflow rate of $200 \text{ m}^3/\text{year}$ (1.1×10^7 moles/year). About 8×10^6 moles of aluminum will be emplaced in each panel and thus aluminum corrosion could continue for 2 years. Based on the reaction enthalpy shown in Table 1, aluminum corrosion will generate a thermal load of about 51 kW. Wang (1996) estimated the maximum temperature that could be generated by aluminum corrosion within a panel to be about 6°C .

2.5 Concrete Hydration

Concrete hydration reactions will occur in the seals and panel closures and in the waste.

2.5.1 Seals and panel closures

Concrete hydration reactions are known to proceed for extended periods (perhaps thousands of years). However, the rates of these reactions decrease with time and, within the WIPP, the greatest evolution of heat will occur during the short periods following emplacement of panel closures during the operational phase and following shaft seal emplacement and repository closure. A quantitative analysis of the thermal effects of emplacing large concrete seals in salt at the WIPP was made by Loken (1994), Loken and Chen (1995). Their analysis showed that the energy released by the hydration of the seal concrete could raise the temperature of the concrete to approximately 53°C and that of the surrounding salt to approximately 38°C one week after seal emplacement.

2.5.2 Waste

WIPP waste contains cement which is used to solidify liquids, particulates and sludges. Storz (1996) estimated that all the waste to be emplaced at the WIPP will contain a total of about 8.5×10^6 kg of cement. This is equivalent to about 1.5×10^7 moles of calcium oxide (CaO) per waste disposal panel, representing the cement as CaO. Although a substantial amount of hydration may occur prior to waste disposal, this process will continue at a slower rate after disposal. Disregarding the hydration that will occur prior to disposal and assuming a brine inflow rate of $200 \text{ m}^3/\text{year}$, the reaction rate of concrete hydration in the panel will be about 1.1×10^7 moles/year, and the reaction could continue for about 1.4 years. Based on the reaction enthalpy shown in Table 1, concrete hydration will generate a thermal load of about 23 kW. Thus, using analyses similar to that used by Wang (1996) the maximum temperature that could be generated by concrete hydration of the waste within a panel is about 2°C .



3.0 Heat From Radioactive Decay

Radioactive decay of the contact handled CH and remote handled RH TRU waste emplaced in the repository will generate heat. The importance of heat from radioactive decay depends on the effects that the induced temperature changes would have on mechanics, fluid flow, and geochemical processes. For example, temperature increases could result in thermally induced fracturing, regional uplift, or thermally driven flow of gas and brine in the vicinity of the repository.

According to the Waste Acceptance Criteria (WAC), the design basis for the WIPP requires that the thermal loading does not exceed 10 kilowatts per acre. The WAC also require that the thermal power generated by waste in an RH TRU container shall not exceed 300 watts, but the WAC do not limit the thermal power of CH TRU waste containers.

A numerical study to calculate induced temperature distributions and regional uplift is reported in DOE (1980, pp.9-149-9-150). This study involved estimation of the thermal power of CH TRU waste containers. The DOE (1980) analysis assumed:

- All CH TRU waste drums and boxes contain the maximum permissible quantity of plutonium. According to the WAC, the fissionable radionuclide content for CH TRU waste containers shall be no greater than 200 grams per 0.21 cubic meter drum and 350 grams per 1.8 cubic meter standard waste box (in Pu-239 fissile gram equivalents).
- The plutonium in CH TRU waste containers is weapons grade material producing heat at 0.0024 watts per gram. Thus, the thermal power of a drum is approximately 0.5 watts and that of a box is approximately 0.8 watts.
- Approximately 3.7×10^5 cubic meters of CH TRU waste are distributed within a repository enclosing an area of 7.3×10^5 square meters. This is a conservative assumption in terms of quantity and density of waste within the repository, because the maximum capacity of the WIPP is 1.756×10^5 cubic meters for all waste (as specified by the Land Withdrawal Act [LWA]) to be placed in an enclosed area of approximately 5.1×10^5 square meters.
- Half of the CH TRU waste volume is placed in drums and half in boxes so that the repository will contain approximately 9×10^5 drums and 10^5 boxes. Thus, a calculated thermal power of 2.8 kilowatts per acre (0.7 watts per square meter) of heat is generated by the CH TRU waste.



- Insufficient RH TRU waste is emplaced in the repository to influence the total thermal load.

Thorne and Rudeen (1980) estimated the long-term temperature response of the disposal system to waste emplacement. Calculations assumed a uniform initial power density of 2.8 kilowatts per acre (0.7 watts per square meter) which decreases over time. Thorne and Rudeen (1980) attributed this thermal load to RH TRU waste, but DOE (1980), more appropriately, attributed this thermal load to CH TRU waste based on the assumptions listed above. Thorne and Rudeen (1980) estimated the maximum rise in temperature at the center of a repository to be 1.6°C at 80 years after waste emplacement.

Sanchez and Trelue (1996) estimated the maximum thermal power of an RH TRU waste container. The Sanchez and Trelue (1996) analysis involved inverse shielding calculations to evaluate the thermal power of an RH TRU container corresponding to the maximum permissible surface dose; according to the WAC the maximum allowable surface dose equivalent for RH TRU containers is 1000 rem/hr. The following calculational steps were taken in the Sanchez and Trelue (1996) analysis:

- Calculate the absorbed dose rate for gamma-ray radiation corresponding to the maximum surface dose equivalent rate of 1000 rem/hr. Beta and alpha radiation are not included in this calculation because such particles will not penetrate the waste matrix or the container in significant quantities. Neutrons are not included in the analysis because, according to the WAC, the maximum dose rate from neutrons is 270 mrem/hr, and the corresponding neutron heating rate will be insignificant.
- Calculate the exposure rate for gamma radiation corresponding to the absorbed dose rate for gamma radiation.
- Calculate the gamma flux density at the surface of a RH TRU container corresponding to the exposure rate for gamma radiation. Assuming the gamma energy is 1.0 MeV the maximum allowable gamma flux density at the surface of a RH TRU container is about 5.8×10^8 gamma rays per square centimeter per second.
- Determine the distributed gamma source strength, or gamma activity, in an RH container from the surface gamma flux density. The source is assumed to be shielded such that the gamma flux is attenuated by the container and by absorbing material in the container. The level of shielding depends on the matrix density. Scattering of the gamma flux, with loss of energy, is also accounted for in this calculation through inclusion of a gamma buildup factor.



The distributed gamma source strength is determined assuming a uniform source in a right cylindrical container. The maximum total gamma source (gamma curies) is then calculated for a RH TRU container containing 0.89 cubic meters of waste. For the waste of greatest expected density (about 6,000 kilograms per cubic meter) the gamma source is about 2×10^4 curies per cubic meter.



Calculate the total curie load of a RH TRU container (including alpha and beta radiation) from the gamma load. The ratio of the total curie load to the gamma curie load was estimated through examination of the radionuclide inventory presented in the WIPP Baseline Inventory Report (BIR) (DOE, 1995). The gamma curie load and the total curie load for each radionuclide listed in the WIPP BIR were summed. Based on these summed loads the ratio of total curie load to gamma curie load of RH TRU waste was calculated to be 1.01.

- Calculate the thermal load of a RH TRU container from the total curie load. The ratio of thermal load to curie load was estimated through examination of the radionuclide inventory presented in the WIPP BIR (DOE, 1995). The thermal load and the total curie load for each radionuclide listed in the WIPP BIR were summed. Based on these summed loads the ratio of thermal load to curie load of RH TRU waste was calculated to be about 0.0037 watts/curie. For a gamma source of 2×10^4 curies per cubic meter the maximum permissible thermal load of a RH TRU container is about 70 watts per cubic meter. Thus, the maximum thermal load of a RH TRU container is about 60 watts, and the WAC upper limit of 300 watts will not be achieved.

Note that Sanchez and Trellue (1996) calculated the average thermal load for a RH TRU container to be less than 1 watt. Also, the total RH TRU heat load is less than 10% of the total heat load in the WIPP. Thus, the total thermal load of the RH TRU waste will not significantly affect the average rise in temperature in the repository resulting from decay of CH TRU waste.

Temperature increases will be greater at locations where the thermal power of a RH TRU container is 60 watts, if any such containers are emplaced. Sanchez and Trellue (1996) estimated the temperature increase at the surface of a 60 watt RH TRU waste container. Their analysis involved solution of a steady-state thermal conduction problem with a constant heat source term of 70 watts per cubic meter. These conditions represent conservative assumptions because the thermal load will decrease with time as the radioactive waste decays. The temperature increase at the surface of the container was calculated to be about 3°C.

In summary, analysis has shown that the average temperature increase in the WIPP repository due to radioactive decay of the emplaced CH and RH TRU waste will be about 1.6°C, with a maximum rise occurring at the center of the repository at about 80 years after waste emplacement. Temperature increases of about 3°C may occur in the vicinity of RH TRU containers with the highest allowable thermal load of about 60 watts (based on the maximum allowable surface dose equivalent for RH TRU containers).

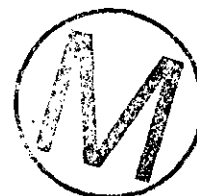


4.0 Conclusions

Heat from exothermic reactions and radioactive decay will result in minor temperature increases in the repository. The potential temperature increases caused by these processes are summarized in Table 2.

Table 2. Maximum temperature increases at the WIPP.

Heat Source	Maximum temperature increase	Time of maximum temperature increase
Backfill hydration	4.5°C	20 years after a drilling intrusion
Backfill carbonation	0.6°C	125 years after a drilling intrusion
Microbial degradation	0.8°C	120 years after a drilling intrusion
Aluminum corrosion	6.0°C	2 years after a drilling intrusion
Concrete hydration (seals)	25°C in the shaft seal 10°C in the surrounding salt	1 week after emplacement
Concrete hydration (waste)	2.0°C	1.4 years after a drilling intrusion
Radioactive decay of CH TRU waste	1.6°C	80 years after disposal
Radioactive decay of RH TRU waste	3°C near a few containers	Within 100 years after disposal



During the operational phase and soon after disposal concrete hydration in the panel closures and shaft seals will give rise to temperature increases lasting a few decades. Heat from radioactive decay will generate a maximum temperature increase of less than 2°C within 100 years after disposal. A number of potential exothermic reactions have been identified. These reactions are brine limited and will cause only minor perturbations to the temperature distribution within the disposal system. The maximum calculated rate of brine inflow to a waste disposal panel occurs for the S2 scenario involving an E1 drilling event at 350 years after disposal. The maximum temperature that could be achieved in the panel

occurs as a result of aluminum corrosion; this reaction could result in a maximum temperature increase of about 6°C two years after the drilling event. Similarly, rapid backfill hydration could result in a maximum temperature increase of less than 5°C. These predicted values of temperature increase are based on a number of conservative assumptions. For example, the calculated temperature resulting from aluminum corrosion is based on the assumption that no corrosion has occurred prior to the drilling event and that all the brine introduced to the waste panel is available for aluminum corrosion. In reality some aluminum corrosion is likely to have occurred prior to the drilling event, reducing the volume of aluminum available for the reaction, and other reactions with lower reaction enthalpies or lower reaction rates will consume brine resulting in a smaller temperature increase.

Temperature increases of the magnitude and duration shown in Table 2 will have no significant effects on the performance of the disposal system. The effects of such temperature increases on the performance of the disposal system have been discussed in the SNL Summary Memos of Record RNT-24 (thermochemical effects), S-10 and GG-4 (thermal convection), S-11, SP-6, RM-1 (thermally-induced stress).



5.0 References

DOE (U.S. Department of Energy), 1980. *Final Environmental Impact Statement, Waste Isolation Pilot Plant*. DOE/EIS-0026. Vol. 1 of 2. U.S. Department of Energy, Washington, DC.

DOE (U.S. Department of Energy) 1995. *Transuranic Waste Baseline Inventory Report*. DOE/CAO-95-1121, Revision 2, December 1995, Carlsbad, NM.

Drever, J.I. 1982. *The Geochemistry of Natural Water*. Prentice-Hall.

Grenthe, I. Fuger, J., Konings, R.J.M., Lemire, R.J., Muller, A.B., Nguyen-Trung, C., and Wanner, H. 1992. *Chemical Thermodynamics of Uranium*. Eds. H. Wanner and I. Forest. Amsterdam, London, New York: North-Holland for NEA/OECD. pp: 30-50.

Krauskopf, K.B. 1982. *Introduction to Geochemistry. Second (International) Edition*. McGraw-Hill International Series in the Earth and Planetary Sciences. McGraw-Hill Book Company. p. 561.

Lide, D.R. 1994. *Handbook of Chemistry and Physics*. CRC Press.

Loken, M.C. 1994. "SMC Thermal Calculations", RSI Calculation No. A141-GE-05, Prepared for Parsons Brinckerhoff, San Francisco, CA. Rapid City, SD: RE/SPEC Inc.

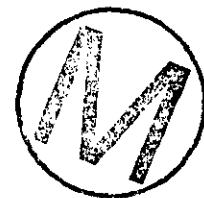
Loken, M.C., and Chen, R. 1995. "Rock Mechanics Analysis of SMC", RSI Calculation No. A141-GE-07, Prepared for Parsons Brinckerhoff, San Francisco, CA. Rapid City, SD: RE/SPEC Inc.

Sanchez, L. C., and Trelue, H. R., 1996. "Estimation of Maximum RH-TRU Thermal Heat Load for WIPP." Memo to T. Hicks (Galson Sciences Ltd.), January 17, 1996. Sandia National Laboratories, Albuquerque, NM. SWCF-A WBS:1.1.6.2.:PA:PBWAC - WIPP ACTIVITY.

Storz, L. 1996. *Estimate of the Amount of Ca(OH)₂ Contained in the Portland Cement Fraction of the Waste for Disposal in the WIPP*. Memo of June 24, 1996. SWCF (Or. 6752), WBS 1.1.09.

Thorne, B. J., and Rudeen, D. K., 1980. *Regional Effects of TRU Repository Heat*. SAND-7161. Sandia National Laboratories, Albuquerque, NM.

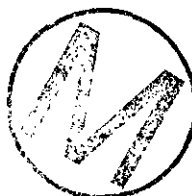
Wagman, D.D., Evans, W.H., Parker, V.B., Schumm, R.H., Halow, I., Bailey, S.M.,



Churney, K.L, and Nuttall, R.L. 1982. The NBS Tables of Chemical Thermodynamic Properties. Selected Values for Inorganic and C₁ and C₂ Organic Substances in SI Units. *Journal of Physical and Chemical Reference Data*, Volume 11, Supplement No. 2. American Chemical Society.

Wang, Y. 1996. *Evaluation of the Thermal Effect of Exothermic Chemical Reactions for WIPP Performance Assessment: A Revised Version.* Memorandum of August 19, 1996. SWCF-A (Org. 6352), WBS 1.1.09.1.1(RC). (attached)

Attachment: memorandum of August 19, 1996, by Yifeng Wang, to Distribution. "Evaluation of the Thermal Effect of Exothermic Chemical Reactions for WIPP Performance Assessment: A revised version," Sandia National Laboratories.



Distribution:

MS 1320 J. Nowak (Org. 6831)
MS 1320 R.V. Bynum (Org. 6831)
MS 1328 D.R. Anderson (Org. 6849)
MS 1335 M.S.Y Chu (Org. 6801)
MS 1341 L.H. Brush (Org. 6832)
MS 1341 R.F. Weiner (Org. 6822)
MS 1341 K.W. Larson (Org. 6822)
MS 1341 A.S. Reiser (Org. 6822)
MS 1341 P.N. Swift (Org. 6821)
MS 1330 SWCF-A (Org. 6352), WBS 1.1.09.1(RC) (two copies)

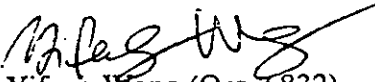


Sandia National Laboratories

Albuquerque, New Mexico 87185-1341

date: August 19, 1996

to: Distribution


from: Yifeng Wang (Org. 6832)

subject: Evaluation of the Thermal Effect of Exothermal Chemical Reactions for WIPP
Performance Assessment: A revised version

Temperature increases caused by exothermal chemical reactions in the repository have been evaluated in the memo by Wang (1996). This memo is the revised version of the previous memo. Two revisions have been made: (1) anoxic steel corrosion reaction is no longer an exothermal reaction; (2) waste panel number is adjusted from eight to ten. All revisions made here do not change the conclusion that the thermal effect of exothermal chemical reactions in the repository is negligible.

Assumptions:

The following exothermal chemical reactions are considered:



Anoxic steel corrosion is a major chemical reaction expected to occur in the repository:



However, this reaction is considered here, because it is not an exothermal reaction. The enthalpy change of Reaction (5) is estimated to be 0.64 Kcal/mole Fe.

Considering that the vertical dimension of the repository (~ 1 m, B. M. Butcher, personal comm.) will be much less than the horizontal extension after room closure, we assume that the heat released from the reactions will be dissipated away mainly from the ceiling and ground of the repository and the heat loss from the side walls is negligible. We also assume that all reactions will take place uniformly in a reaction region of interest. We here restrict the reaction region in a single waste panel, for the following reason: Some of the above reactions may be limited by brine inflow. BRAGFLO simulations have shown that, in the human intrusion cases, the rate of brine inflow into a borehole-penetrated waste panel will be significantly higher than that into the rest of the repository. Choosing a panel rather than the whole repository as a reaction region will make heat generation rate per unit of volume higher and the heat dissipating surface area smaller in our calculations, and

therefore it is conservative. However, this choice will not affect the calculations for the reactions that are not limited by brine inflow, as you will see below.

Theory:

Based on these assumptions, the thermal effect of an exothermal chemical reaction can be modeled by a simplified system shown in Figure 1. The temperature distribution (T) can be described by the following equations:

$$C_p \rho \frac{\partial T}{\partial t} = k \frac{\partial^2 T}{\partial X^2} \quad (6)$$

$$T(X,0) = T_0 \quad (7)$$

$$R\Delta H = 2Sk \left. \frac{\partial T}{\partial X} \right|_{x=0} \quad (8)$$

$$T(\infty, t) = T_0 \quad (9)$$

where C_p is the heat capacity of surrounding rocks (J/mole/K); ρ is the molar density of surrounding rocks (moles/m³); t is time (year); X is the spatial coordinate (m); k is the thermal conductivity of surrounding rocks (J/year/m/K); T_0 is the background temperature (K); R is the reaction rate (moles/year); ΔH is the enthalpy change of the reaction (J/mole); S is the horizontal area of a waste panel (m²).

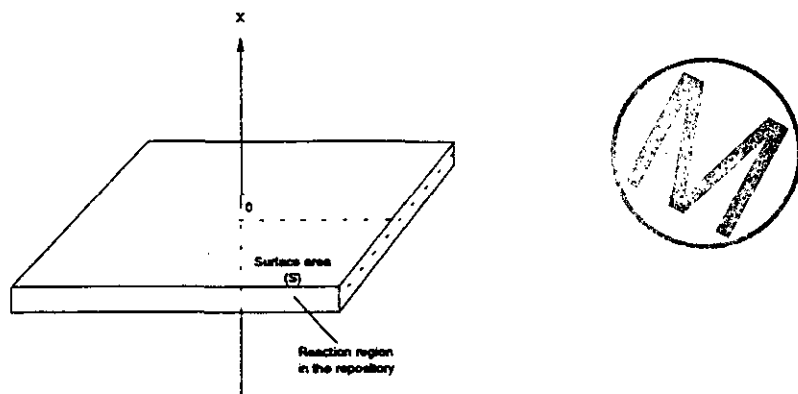


Figure 1. A modeling system for heat production and conduction.

The above equations can be solved for T with a Laplace-transformation method: --

$$T - T_0 = -\frac{R\Delta H}{2S\sqrt{C_p\rho k}} \left[2\sqrt{\frac{t}{\pi}} e^{-\frac{C_p\rho X^2}{4Kt}} - \sqrt{\frac{C_p\rho}{k}} X \operatorname{erfc}\left(\frac{X}{2}\sqrt{\frac{C_p\rho}{kt}}\right) \right]. \quad (10)$$

The temperature increase in the repository (ΔT) is obtained by setting $X = 0$ in equation (6):

$$\Delta T = T(0,t) - T_0 = -\frac{R\Delta H}{S} \sqrt{\frac{t}{\pi C_p\rho k}}. \quad (11)$$

Equation (7) shows that the repository temperature will increase with t until $t = \frac{M}{R}$, when all the reactant is consumed. Here M is the inventory of the reactant in a waste panel (moles). Therefore, the maximum temperature increase (ΔT_{\max}) in the repository due to the exothermal reaction can be calculated by

$$\Delta T_{\max} = T(0,t) - T_0 = -\frac{\Delta H}{S} \sqrt{\frac{RM}{\pi C_p\rho k}}. \quad (12)$$

Equation (12) shows that, for the reactions not limited by brine inflow, reducing the reaction region size does not affect ΔT_{\max} , because the parameters S , R , and M will be reduced by the same factor, which is canceled out in the equation. This is not true for the brine-limited reactions, the rates of which are no longer dependent on reactant inventory.

Assuming the physical properties of the surrounding rocks can be represented by halite, we then have:

$$C_p = 50 \text{ J/mole/K (Lide, 1994, p. 12-158)}$$

$$\rho = 3.7 \times 10^4 \text{ moles/m}^3 \text{ (Lide, 1994, p. 4-149)}$$

$$k = 6 \text{ W/m/K} = 1.9 \times 10^8 \text{ J/year/m/K (Lide, 1994, p. 12-165)}$$

$$S = 1.2 \times 10^4 \text{ m}^2 \text{ (Sandia WIPP Project, 1992, p. 3-4).}$$

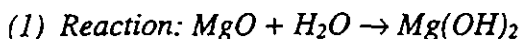
With these parameter values, we obtain from equation (12):



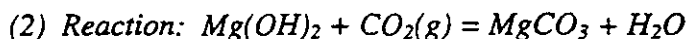
$$\Delta T_{\max} = 2.5 \times 10^{-12} \Delta H \sqrt{RM} \quad (13)$$



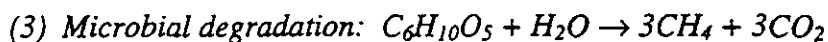
Results:



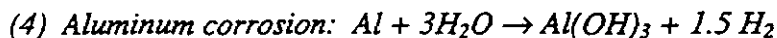
We assume that this reaction is instantaneous and thus is limited by brine inflow. Based on BRAGFLO simulations for E1 scenario (Figure 2), the conservative (maximum) estimate of the rate of brine inflow into a borehole penetrated waste panel is about 200 m³/year, equivalent to the reaction rate of 1.1x10⁷ moles/year. With $\Delta H = -3.9 \times 10^4$ J/mole (Drever, 1982, p. 351-356) and $M = 2 \times 10^8$ moles, we estimate $\Delta T_{\max} \approx 4.5$ K.



We assume that this reaction is limited by microbial CO₂ production. It is estimated that the maximum rate of CO₂ production (R) is 2.9x10⁵ moles/year and the total CO₂ that can be produced (M) is 3.6x10⁷ moles in a single waste panel (Wang & Brush, 1996; DOE/CAO, 1996). With $\Delta H = -0.8 \times 10^5$ J/mole (Drever, 1982, p. 351-256), ΔT_{\max} is estimated to be 0.6 K.

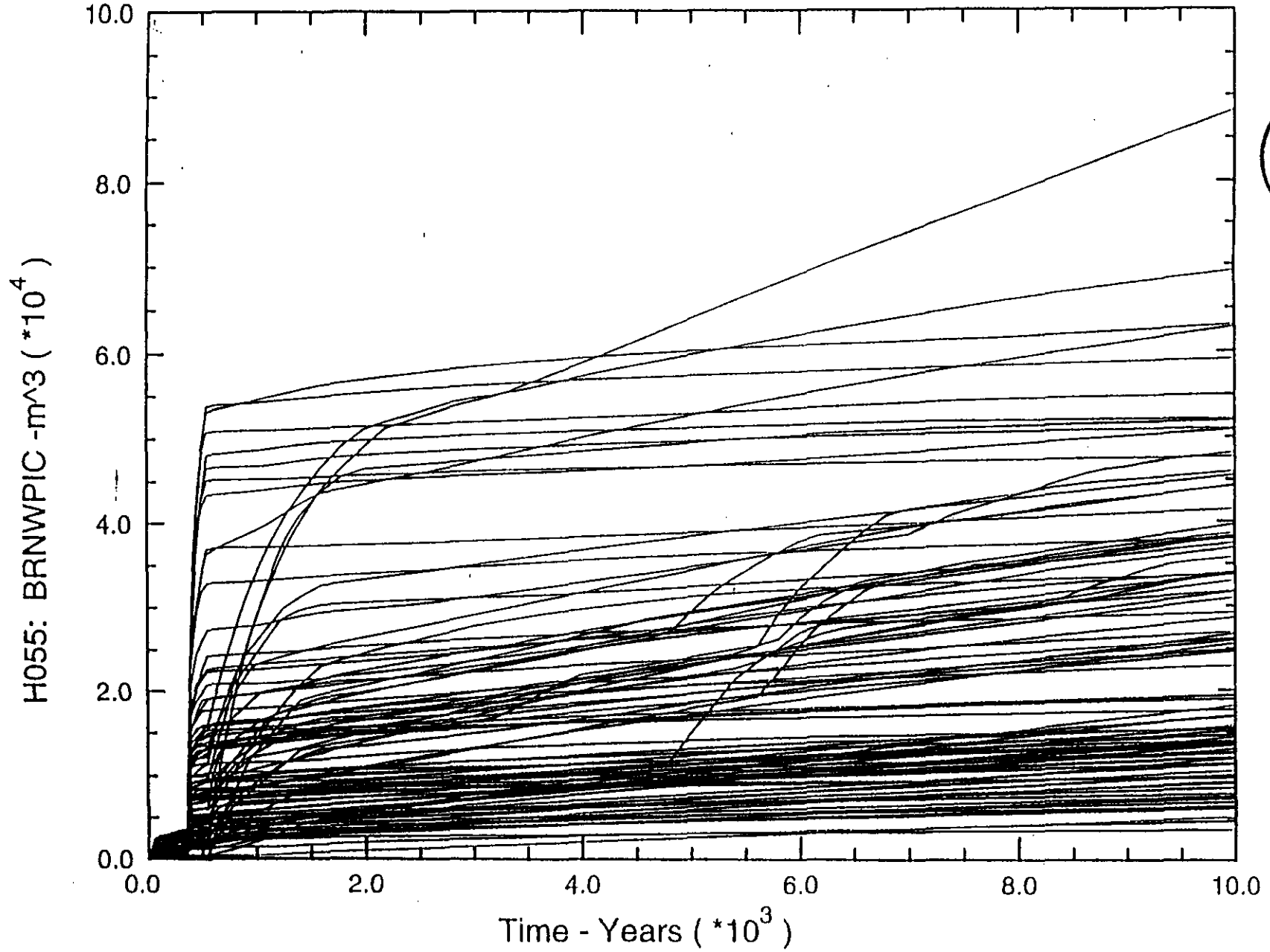


The maximum reaction rate and the inventory of C₆H₁₀O₅ in a single waste panel are estimated to be 1x10⁵ moles/year and 1.2x10⁷ moles (Wang & Brush, 1996; DOE/CAO, 1996). With $\Delta H = -3.1 \times 10^5$ J/mole (Lide, 1994, p. 5-16 to 5-37), ΔT_{\max} is estimated to be 0.8 K. Because of lack of thermodynamic data for cellulose materials, we here assume that the enthalpy of C₆H₁₀O₅ is approximately equal to that of C₆H₁₀O₄.



The inventory of Al in a single panel is about 8x10⁶ moles (DOE/CAO, 1996). Aluminum are present as foil in the waste and its thickness is estimated to be 2.54x10⁻⁴ cm. The total surface area of Al foil is thus estimated to be ~ 2.6x10⁸ m². With this high surface area and the measured corrosion rate (2.9 mole H₂/m²/year, Telander & Westerman, 1996), Al corrosion reaction is expected to be limited by brine inflow, and the maximum corrosion rate is ~ 0.4x10⁷ moles/year. With $\Delta H = -4.4 \times 10^5$ J/mole (Drever, 1982, p. 351-356), ΔT_{\max} is estimated to be 6 K.

Cumulative Brine Inflow into Waste Panel

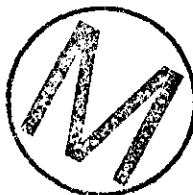


The two brine-inflow-limited reactions - MgO hydration and Al corrosion - could possibly bring repository temperature up to 6 K. However, this temperature increase will not affect the overall repository performance, for two reasons: (1) The maximum temperature, if it is achieved, will be sustained only over a very short time period. For example, to achieve this temperature, Al has to be corroded completely within 2.5 years. After that, the accumulated heat will be dissipated away quickly. Thus, the maximum temperature, if it is attained, will last perhaps less than a year. (2) More importantly, because the two reactions are brine-limited, they will consume all free brine in the repository until all the reactants are completely consumed. Therefore, the maximum temperature will occur much earlier than enough free brine accumulates in the repository for the release of dissolved actinides. Based on the above calculations, the thermal effect of the other reactions, which are not limited by brine inflow and can last over a significant portion of 10000 year time period, are definitely negligible.

In conclusion, ignoring the thermal effect of chemical reactions (1 - 5) can not affect the overall repository performance assessment.

References:

- DOE/CAO (1996) Transuranic Waste Baseline Inventory Report (Rev. 3).
Drever, J. I. (1982) The Geochemistry of Natural Water. Prentice-Hall.
Lide, D. R. (1994) Handbook of Chemistry and Physics. CRC Press.
Sandia WIPP Project (1992) Preliminary Performance Assessment for the Waste Isolation Pilot Plant, December 1992. Volume 3: Model Parameters. SAND92-0700/3.
Telander, M. R. & Westerman R. E. (1996) Hydrogen Generation by Metal Corrosion in Simulated Waste Isolation Pilot Plant Environments: Final Report. (Draft)
Wang, Y. & Brush, L. H. (1996) Estimate of gas-generation parameters for the long-term performance assessment. memo to M. S. Tierney, 1/26/1996, WBS 1.1.09.1.1(RC).
Wang, Y. (1996) Evaluation of the Thermal Effect of Exothermal Chemical Reactions for WIPP Performance Assessment. memo to V. R. Bynum & L. H. Brush, 7/19/1996, WBS 1.1.09.1.1(RC).



Distribution:

MS 1320 J. Nowak (Org. 6831)
MS 1320 R. V. Bynum (Org. 6831)
MS 1328 D. R. Anderson (Org. 6849)
MS 1335 M. S. Y. Chu (Org. 6801)
MS 1341 J. T. Holmes (Org. 6832)
MS 1341 L. H. Brush (Org. 6832)
MS 1341 Y. Wang (Org. 6832)
MS 1341 R. F. Weiner (Org. 6822)
MS 1341 K. W. Larson (Org. 6822)
MS 1341 A. S. Reiser (Org. 6822)
MS 1330 SWCF-A (Org. 6352), WBS 1.1.09.1.1(RC)

